Acoustic Detection for Warning of Drowning Accidents

Frederik Sidenius Dam

Acoustics and Audio Technology, Group 1076, Spring 2023

Master's Thesis

STUDENT REPORT

AALBORG UNIVERSITY

Written in LaTeX and compiled with pdfLaTeX in Overleaf. Body text is written in 10pt Inter Light font. Sketches and diagrams are made using diagrams.net. Plots are generated using Matplotlib and REW. Schematics and layouts are designed using EasyEDA Online Editor.

AALBORG UNIVERSITY
STUDENT REPORT

Department of Electronic Systems
Aalborg University
https://www.es.aau.dk

Title:
Acoustic Detection for Warning of Drowning Accidents

Type:
Master's Thesis

Project Period:
February 2023 - June 2023

Project Group:
1076

Student:
Frederik Sidenius Dam

Supervisor:
Flemming Christensen

Page Numbers: 74 (including appendices)

Date of Completion:
1st June 2023

Abstract:

Drowning accidents in harbours present a significant challenge, necessitating effective preventive measures. This project investigates the feasibility of employing hydrophones for capturing underwater sounds to provide early warnings of such accidents within a cost-effective system. Through comprehensive problem analysis and on-site measurements in various harbour environments, valuable insights into underwater acoustics and the capabilities of hydrophones are gained. The research findings demonstrate the viability of inexpensive custom hydrophones as reliable acoustic sensors, offering promising capabilities compared to calibrated reference hydrophones. Furthermore, the study highlights potential issues associated with the prototype hydrophones, such as high inherent noise levels and low-frequency roll-off. Additionally, the development of the suggested algorithm, for recognising and locating sound sources, is left for future endeavours. The results lay the foundation for further research to optimise and refine the developed prototypes and integrate these into the proposed system with existing safety infrastructure. Ultimately, the conclusions drawn from this research provide great potential for enhancing safety measures and potentially reducing the number of drowning accidents in harbours.

Contents

Preface

This thesis is written during the 4th semester of the Master's programme in Signal Processing and Acoustics with the Acoustics and Audio Technology specialisation at Aalborg University.

It is intended to be read chronologically as presented in the table of contents and the appendices are included as supporting information and referenced continuously throughout the report. Appendices include documentation of laboratory and field measurements and recorded audio files are provided in an external attachment folder.

Citations follow the IEEE referencing style and are listed sequentially in the bibliography based on the order cited. All figures, tables and equations are uniquely numbered and referenced in the text when applicable. Figures are produced by the author except when a citation is provided in the caption.

The author would like to thank Assistant Engineers Claus Vestergaard Skipper, Kenneth Knirke and Ben Klauman Krøyer for making calibration couplers, assistance with equipment and general support in the laboratories.

With the signature below, I confirm to have written the full report and provided citations to external material when applicable.

Aalborg University, 1st June 2023

Frederik Sidenius Dam
fdam21@student.aau.dk
20211693

Part I

Report

1 Introduction

At least 70 people drowned in Denmark in 2021, and if statistically corrected for missing reports, this number rises to about 90 [1]. Of the reported drowning accidents, 15 of them happened in harbours, a number that reached more than 20 in 2022. For unknown reasons, these are large increases from the 10-year average of 11 people from 2011-2020 [2].

In a review of all drowning accidents from 2001 to 2018 made by the Danish philanthropic organisation TrygFonden, 174 fatalities are linked to harbours. Harbours are often located nearby city centres and in 114 of these accidents, alcohol was involved. Increased awareness has led to new preventive initiatives, where in addition to rescue ladders, fencing and increased lighting, both Aalborg and Aarhus municipalities are using thermal cameras with automatic warning of the emergency services [3]. With the recent implementation of these initiatives, zero reports of drowning accidents and a halving of rescue operations is seen in Aarhus by the end of 2022. However, despite new initiatives and favourable statistics, the problem is not believed to be solved [4].

While fencing has been a part of the solution in Aarhus this is not welcomed as a feasible solution everywhere. In Aalborg, the comprehensiveness, false sense of security and people balancing on the bridge railing as a test of manhood are among the strongest arguments against [5]. Thermal cameras currently monitor approximately 200 meters of the harbourfront in Aalborg, but despite being life-saving in two cases, the technology fails due to the limited field of view. Having around two kilometres of critical waterfront with increased risk, the cost of setting up the required ten additional cameras is estimated at two million DKK [6].

This project proposes a novel approach to prevent drowning accidents by utilising underwater microphones, known as hydrophones, as key components in an acoustic detection system.

1.1 Motivation

The act of listening to sounds in the water can be traced back many years beginning with the following notebook quotation [7]:

> *"If you cause your ship to stop, and place the head of a long tube in the water and place the outer extremity to your ear, you will hear ships at a great distance from you."* - Leonardo da Vinci, 1490

Methods and equipment using sound for transmitting and receiving information under the surface of the water have seen remarkable advances throughout the years. Historically it has been used in many cases to navigate, measure distances and detect objects for both military and nonmilitary purposes. A collective term for these techniques is sound navigation and ranging (SONAR) [7].

Additional motivation comes from the author's experiences as a scuba diving professional. Here underwater sounds are used to communicate in case of bad visibility or to get the attention of other divers when out of sight or at a distance.

Human hearing in water has lower sensitivities than in air and shows inferior directional abilities, indicating that humans are not adapted for underwater hearing [8]. However, transducers can be optimised for picking up underwater sound and custom hydrophones constructed relatively inexpensively as seen in several do it yourself (DIY) solutions, e.g. [9].

1.2 Problem Analysis

Overall the underwater acoustic environment is somewhat complicated regarding both sound propagation and ambient noise. This makes signal detection challenging which is the focus of the following sections beginning with an analysis of the selected case harbours.

1.2.1 Specific Cases

The two largest cities in Jutland are chosen for case studies. Both cities have large harbourfronts with a history of multiple drowning accidents and are actively involved in prevention efforts, as highlighted in the introduction. A short description alongside an analysis of critical parameters is provided for each case.

Aalborg

Aalborg is the fourth largest city in Denmark and is located inland in the northern part of Jutland. However, the city is connected to both the North Sea and Kattegat by the Limfjord. Saltwater is led to the Limfjord from the North Sea (salinity of 32 to 34 ‰) and Kattegat (salinity of 19 to 25 ‰) as well as freshwater from the catchment area [10]. Water temperatures varies from 1.8 to 19.3 °C with a yearly average of 10.2 °C [11]. The tidal range in 2023 is predicted to be 41 cm, but the actual sea level variations measured are larger due to meteorological and oceanographic fluctuations [12]

The Limfjord has a depth of around 2 to 10 m at Aalborg with some exceptions of extremities up to 15.8 m, according to the nautical chart in Fig. 1.1. Its seabed consists of mud and sand with the majority being sandy mud [13]. Besides several marinas, the commercial waterfront areas are owned by the Port of Aalborg and Aalborg Portland, with a total of 1192 ships calling at the ports in 2021 [14].

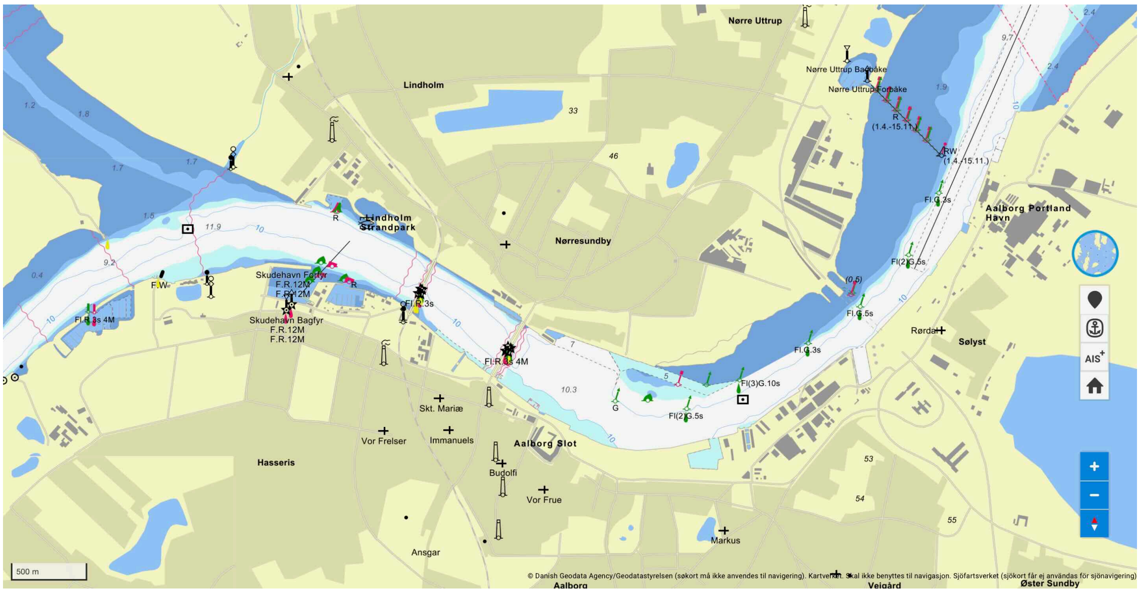

Figure 1.1: Nautical chart of the Limfjord in Aalborg [15].

Aarhus

Aarhus is the second largest city in Denmark and is located on the eastern shore of Central Jutland in the Kattegat. The seawater, with a salinity of 18 to 30 ‰ most part of the year, is a mixture of saltwater from the Skagerrak and brackish water from the Baltic Sea [10]. Water temperatures varies from 0.3 to 20.8 °C with a yearly average of 9.9 °C [11]. The tidal range in 2023 is predicted to be 62 cm, but the measured actual sea level variations are larger due to meteorological and oceanographic fluctuations [12]

Aarhus harbour basin has a depth from around 2 to 11 m, according to the nautical chart in Fig. 1.2. Its seabed consists mainly of till; a mixed sediment type of glacial origin [13]. Besides several marinas, the commercial area is owned by the Port of Aarhus with a total of 6362 ships calling at the port in 2021 [14]. Additionally, a new neighbourhood, Aarhus Docklands (in Danish: Aarhus Ø), began construction in 2008 and here in 2023 it is a vibrant part of the city, completely surrounded by water [16].

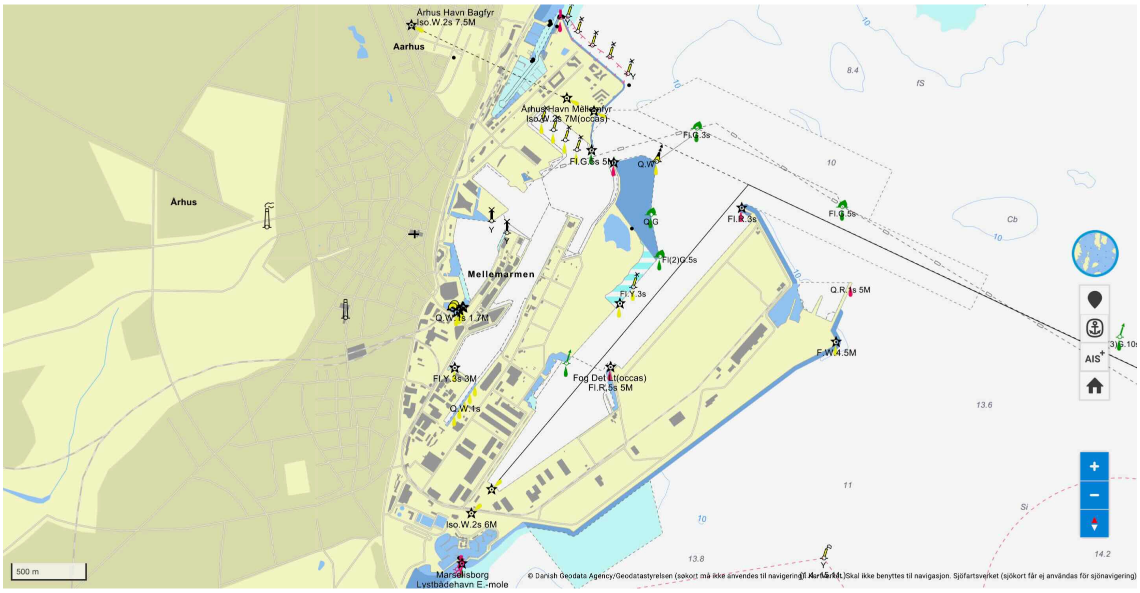

Figure 1.2: Nautical chart of the harbour basins in Aarhus [15].

1.2.2 Sound Propagation in Water

Sound propagates in fluids with a *specific acoustic impedance* that is a ratio of sound pressure and particle speed

$$\mathbf{z} = \frac{\mathbf{p}}{\mathbf{u}} \tag{1.1}$$

where

$\mathbf{z}$	=	specific acoustic impedance	[Pa s/m]
$\mathbf{p}$	=	acoustic pressure	[Pa]
$\mathbf{u}$	=	particle velocity	[m/s]

For a plane wave, ignoring the spherical spreading, this becomes a real value

$$\mathbf{z} = r = \rho c \tag{1.2}$$

where

r	=	specific acoustic resistance	[Pa s/m]
ρ	=	fluid density	[kg/m^3]
c	=	speed of sound	[m/s]

The product ρc is often called the *characteristic impedance* since it is a characteristic property of the medium. For air (1 atm) at 20 °C this is

$$\rho c \approx 415 \, \frac{\text{Pa s}}{\text{m}}$$

and for seawater at 13 °C it is

$$\rho c \approx 1.54 \times 10^6 \, \frac{\text{Pa s}}{\text{m}}$$

At the boundary between two different media, some of the sound energy is reflected, and some is transmitted, with the amount depending on their relative characteristic impedance [17].

Reflection and Transmission

For a plane wave at normal incidence, the *reflection coefficient* is given by

$$\mathbf{R} = \frac{\mathbf{P}_r}{\mathbf{P}_i} = \frac{r_2 - r_1}{r_2 + r_1} \tag{1.3}$$

where

$\mathbf{R}$	=	reflection coefficient	[-]
$\mathbf{P}_r$	=	complex acoustic pressure amplitude of the reflected wave	[Pa]
$\mathbf{P}_i$	=	complex acoustic pressure amplitude of the incident wave	[Pa]
r_1	=	characteristic acoustic impedance of the first medium	[Pa s/m]
r_2	=	characteristic acoustic impedance of the second medium	[Pa s/m]

The large difference in impedance between air and water makes this a highly reflective boundary, and with the values given previously for air and seawater, the reflection coefficient becomes

$$\mathbf{R} = \pm 0.999 \tag{1.4}$$

where $|\mathbf{R}| = 1$ is full reflection and $|\mathbf{R}| = 0$ is full transmission (when $r_1 = r_2$).

Surface-, bottom-, and other boundary-reflected waves may combine with the direct wave in the case of a non-directional sound source. Interference then causes the sound waves to either reinforce or partially cancel each other, depending on their relative phases. This phenomenon is more pronounced in shallow water where the reflected waves travel shorter distances between the source and receiver. Artificial constructions as well as natural banks, e.g. in harbours, canals or streams, increase the number of reflections and thereby the complexity of the sound propagation. The combination of all these reflected waves creates a persistence of sound called reverberation.

Specular reflections occur when a surface is relatively smooth compared to the wavelength, however, if this is not the case the reflections will be diffuse. This scattering of sound waves may also occur from other inhomogeneities such as fish, bubbles or particulate matter. However, wavelengths are relatively long in seawater (75 m to 75 mm), within the audible frequency range (20 Hz to 20 kHz), compared to air (17.15 m to 17.15 mm). This is due to the higher speed of sound in salt water, generally referenced at 1500 m/s, which is more than four times higher than in air (343 m/s) [17].

Speed of Sound and Refraction

The speed of sound in freshwater depends on the ambient temperature and hydrostatic pressure (depth), whereas in seawater it also depends on salinity. All of these factors exhibit diurnal and seasonal variations.

Inhomogeneities in temperature, pressure, and salinity induce spatial variations in sound speed. This causes a bending of the sound waves (refraction), a phenomenon most pronounced in the vertical direction (with varying depth). Variations in salinity are important near the surface where the effects of rain and evaporation have the largest impact and when waters of differing salinity meet.

In the first 100 m of the ocean, the change in pressure (about 10 atm) causes an insignificant increase in sound speed of 1.6 m/s (about 0.1 %). However, differences of more than 5 °C are common in the same region, and a rise of 5 °C increases the speed of sound by 16 m/s (about 1 %) for temperatures near 15 °C. Seawater freezes a couple of degrees below the freezing point for water (0 °C) depending on the specific salinity.

The ocean can generally be divided into four depth-wise regions. The *deep sound-channel axis* acts as a boundary between the *deep isothermal layer* and *main thermocline*, typically around 1000 m. Above the main thermocline, there is the *seasonal thermocline* followed by the uppermost *surface layer*. The characteristics of the surface layer are influenced by day-to-day and even hour-to-hour environmental variations. In the presence of significant surface-wave activity, this surface layer becomes a *mixed layer*, where pressure is the sole factor impacting the sound speed [17].

Transmission Loss

Transmission loss describes the accumulated decrease of intensity of an acoustic wave and is defined as

$$TL = 10\log\left(\frac{I(1)}{I(r)}\right) = 20\log\left(\frac{P(1)}{P(r)}\right) \tag{1.5}$$

where

TL	=	transmission loss	[dB]
I	=	acoustic intensity	[W/m^2]
P	=	peak acoustic pressure amplitude	[Pa]
r	=	distance from the sound source in meters	[-]

As an example, the pressure amplitude of a damped spherical wave is

$$P(r) = \frac{A}{r}\exp\left(-\alpha(r-1)\right) \tag{1.6}$$

where

A	=	peak acoustic pressure amplitude	[Pa]
α	=	absorption coefficient	[Np/m]

A plane wave has a constant pressure amplitude, but for a spherical wave, the amplitude decreases inversely with the distance from the source ($\approx$ 6 dB for each doubling of distance).

For frequencies such that $\alpha \ll 0.1$ Np/m, (1.5) reduces to

$$TL = 20\log\left(r + ar\right) \tag{1.7}$$

with

$$a = 8.7\alpha \tag{1.8}$$

where

a	=	absorption coefficient	[dB/m]

An example is given in [17] with seawater of pH = 8, salinity = 35 ‰ and temperature = 5 °C, which results in a = 0.063 dB/km at 1 kHz and a = 1.1 dB/km at 10 kHz.

In reality, the geometrical spreading is affected by refraction and interference associated with multipath propagation, and the attenuation from diffraction and scattering influences the general losses [17].

1.2.3 Signal Detection

The critical operation is to detect a desired acoustic signal in the presence of noise. In this case, the sound of a person falling into the water and/or moving inside the water should be recognised and localised. A system using hydrophones to listen for acoustic events is often called a *passive sonar*.

Hydrophones are electroacoustic transducers that convert acoustic energy into electrical energy. There are several characteristics to consider, where sensitivity, bandwidth, and directionality are among the most important.

Ambient sounds vary with the acoustic environment and include everything from human-made to biological, geological, meteorological, and other oceanographic sounds. For instance, the sound of breaking waves could appear similar to, and therefore mask or be confused with the desired sound. Other sounds might solely be background noise, but knowledge of the environmental sounds is essential to improve the signal-to-noise ratio (SNR) and enhance signal detection. Localising the sound source can be crucial to the rescue operation, and this information could be provided with various degrees of accuracy.

1.3 Problem Statement

Drowning accidents are an increasing and important problem, particularly in the frigid waters found within Danish harbours. Based on the introduction and analysis of the specific cases, sound propagation in water and signal detection, the following research question is formulated:

> *Can (inexpensive custom) hydrophones be used for acoustic detection in a system for warning of drowning accidents in harbours?*

2 System Specification

The following sections will delve into a field analysis that draws upon measurements made at the harbours of Aalborg and Aarhus. This is followed by an assessment of functional and non-functional system requirements and the overall delimitations of the project.

2.1 Field Analysis

Building upon the problem analysis in Sec. 1.2, on-site measurements were conducted to enhance the understanding of the distinct acoustic environments, prior to establishing the system requirements. The information presented in this section is derived from the field measurements, which are further documented in Appx. B. These measurements encompass various aspects, including ambient background noise, test jumps, and specific noise sources commonly encountered in Danish harbours.

Since high-frequency tones were observed above 18 kHz, all recordings presented in this section have been low-pass filtered in Audacity 3.3.2 [18]. The purpose of this filtering process is to reduce the presence of the tones and enable more meaningful comparisons among the recordings. However, Appx. B.1 and B.2 contain original visualisations with the full bandwidth. The filter is designed to have a cut-off frequency of 12 kHz and a 24 dB/octave roll-off.

Sound pressure level (SPL) plots are calculated broadband using a fast time weighing of 125 ms. The average SPL of the entire clip is indicated by the dashed line. All spectrograms utilise the same colour scale within a dynamic range of 80 dB. Specific ranges are selected based on a calculated peak, resulting in variations.

The audio clips selected for visualisations in this section can be found in 'Attachments/Field Analysis'. These clips are normalised to a peak amplitude of −6 dBFS for convenient playback. Additionally, the full-length unaltered recordings are available in 'Attachments/Field Measurements/Raw Recordings'.

2.1.1 Background Noise

Background noise levels can be remarkably diverse and undergo variations throughout the day, week, month and year. In an attempt to obtain comprehensive information about background noises, multiple recordings have been made at different locations and times of the day. The first example presents the background noise level recorded in the harbour basin in Aarhus during the day (refer to the picture in Fig. 2.1).

Figure 2.1: Picture from the measurements in Aarhus (day).

This recording contains various natural sounds (e.g. the gentle water movement) and a pulsing tone around 800 Hz from an unknown source. Overall the clip has an average SPL of 78 dB and is a good representation of the general background noise during the measurements. Both SPL and a spectrogram of the recording are shown in Fig. 2.2.

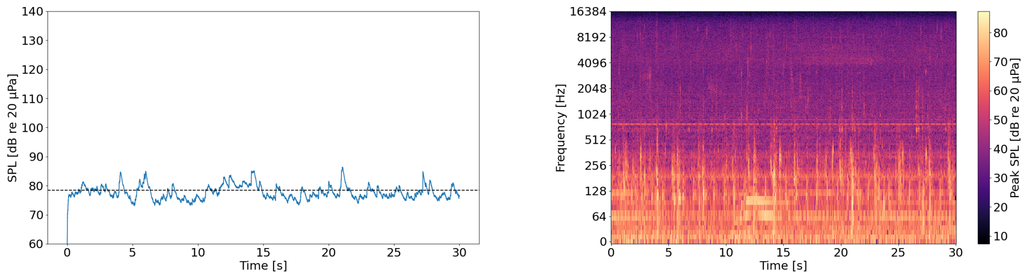

(a) SPL

(b) Spectrogram

Figure 2.2: Recording of the background noise in Aarhus (day).

The second example is background noise measured at the exact same location, but this time during the evening (see the picture in Fig. 2.3).

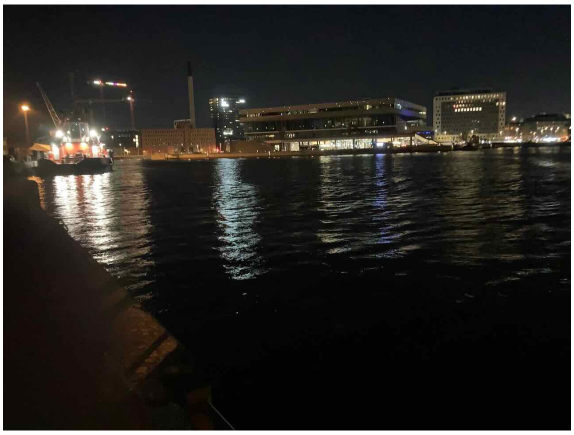

Figure 2.3: Picture from the measurements in Aarhus (evening).

In this recording, there are less movement of the water and the individual natural sounds stand out more. The pulsating tone around 800 Hz is still present which is accompanied by a pure tone around 2400 Hz. In general, with a lower average SPL of 70 dB, this clip is likewise a good representation of the background noise during the measurements. SPL and spectrogram of the recording are shown in Fig. 2.4.

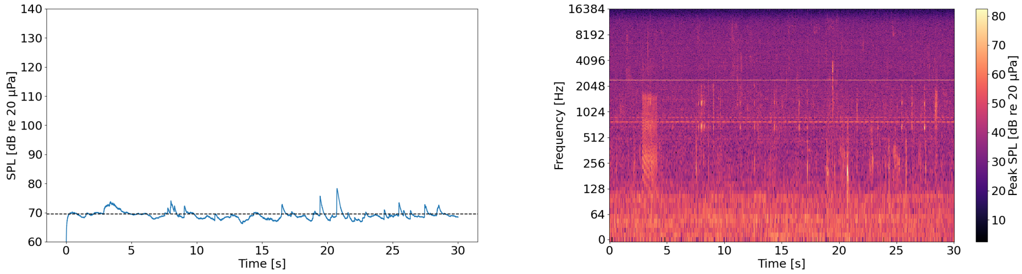

(a) SPL **(b)** Spectrogram

Figure 2.4: Recording of the background noise in Aarhus (evening).

The last example of background noise is measured in Aalborg on a day with significantly higher wind speeds and more waves than in Aarhus (refer to the picture in Fig. 2.5).

Figure 2.5: Picture from the measurements in Aalborg.

The breaking waves are more pronounced in this recording, masking most other natural sounds. However, sounds that could come from a motor are heard, which might be what is visible in the spectrogram as a pulsating tone around 3 kHz. With fairly invariant background noise, the clip provides a fine representation of the measurements in general. As an assumed result of the larger wave activity, the average SPL in this clip is 84 dB. Both SPL and a spectrogram of the recording are shown in Fig. 2.6.

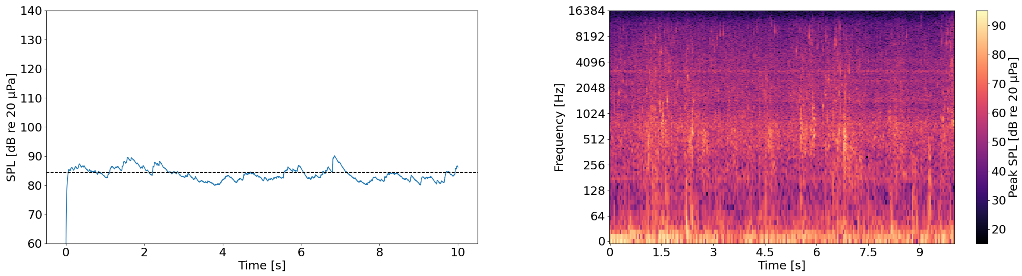

(a) SPL **(b)** Spectrogram

Figure 2.6: Recording of the background noise in Aalborg.

These measurements are, of course, not representative of general background noise levels in harbours, but they provide a good indication of what to expect.

2.1.2 Noise Sources

The presented background noise levels do not include any noticeable dominant noise sources. However, two of these were recorded during the measurements in Aarhus Harbour. Initially, measurements were made of a ferry en route to Samsø, which typically docks at Dokk1 several times a day (see the picture in Fig. 2.7).

Figure 2.7: Picture of the ferry sailing out of the basin.

The ferry docked approximately 200 m away and sailed past the hydrophone at a distance of around 80 to 100 m. This resulted in noise levels exceeding 100 dB SPL, as evident from the plots in Fig. 2.8. Even at a distance, significant noise levels are observed, despite the attenuation of high frequencies. The spectrogram clearly shows that the most prominent sounds are concentrated below 1 kHz, which also dominates the overall broadband SPL.

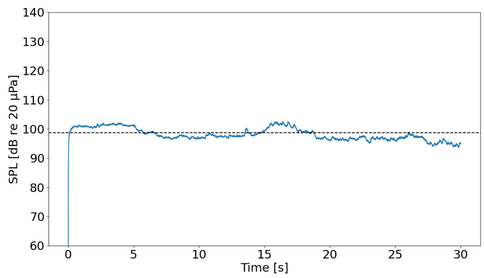

(a) SPL

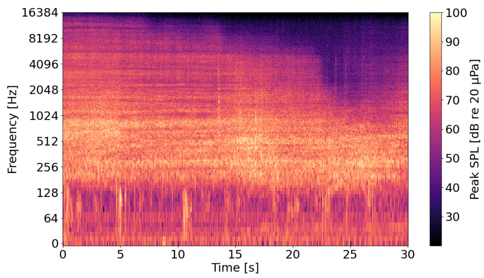

(b) Spectrogram

Figure 2.8: Recording of the ferry sailing out of the basin.

The other loud sound source recorded was a smaller dual-motor speedboat (refer to the picture in Fig 2.9).

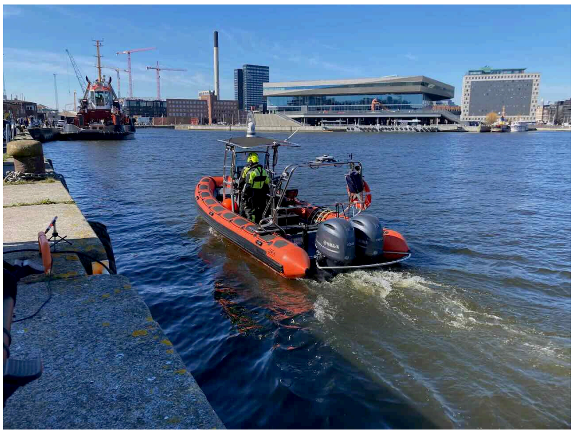

Figure 2.9: Picture of the speedboat sailing close by.

The speedboat was sailing around the perimeter of the harbour basin, and at one point, it passed in close proximity to the hydrophone, with a distance of only a few meters. This resulted in exceptionally high sound pressure levels, reaching nearly 130 dB, peaking at frequencies around 100 Hz, as depicted in Fig. 2.10.

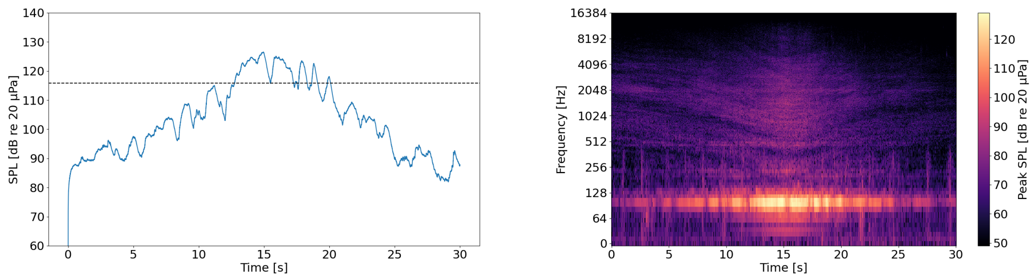

(a) SPL **(b)** Spectrogram

Figure 2.10: Recording of the speedboat sailing close by.

After the speedboat passed, the bow waves, presumably created by the ferry, were captured crashing against the walls of the harbour. These can be seen in Fig. 2.11 as prominent spikes reaching up to 110 dB SPL with the majority of sound energy concentrated below 500 Hz.

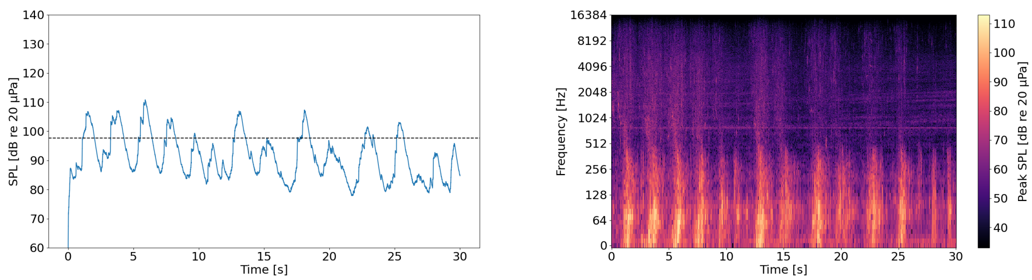

(a) SPL **(b)** Spectrogram

Figure 2.11: Recording of bow waves from the ferry.

Overall, these recorded noise sources increase the background noise levels significantly. However, it is important to note that this selection represents only a small sample of potential noise sources. Other sea vessels may produce different sounds, and factors such as increased wind, larger breaking waves, and heavy rain could likewise contribute to elevated background noise levels.

2.1.3 Desired Sound Sources

The desired sound sources are people falling into the water, and to emulate this scenario, controlled jumps were recorded in Aalborg (see the picture in Fig. 2.12). Two hydrophones were used to simultaneously capture the same splash at different distances. Multiple jumps were recorded and documented in Appx. B.1. However, this section focuses on two specific jumps, resulting in a total of four different distances being represented. Each jump is presented in a short 10 s clip with the person hitting the water around the midpoint.

Figure 2.12: Picture of the test subject before jumping in.

The first example, which is also the closest, is shown in Fig. 2.13. It displays a prominent spike in SPL just below 120 dB. The majority of the sound is concentrated at very low frequencies, but clear peaks can also be observed at higher frequencies. The spectrogram reveals two distinct acoustic events, an observation that is also audible.

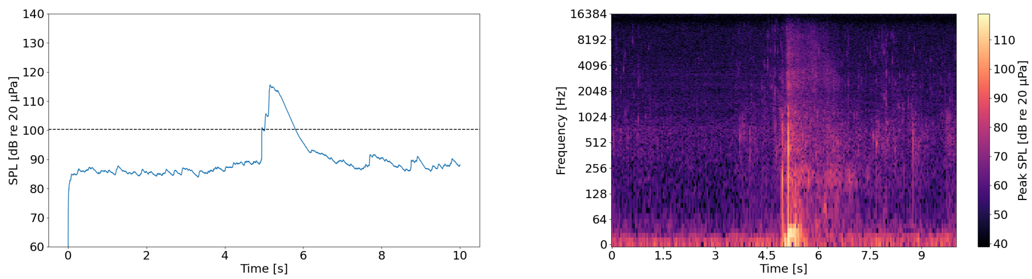

(a) SPL

(b) Spectrogram

Figure 2.13: Recording of the test subject jumping into the water 1 m from hydrophone 1.

The same jump, recorded at a distance of 11.6 m from the second hydrophone, is shown in Fig. 2.14. This time the SPL exhibits only a minor peak, and with careful observation, the splash can both be seen on the spectrogram and heard.

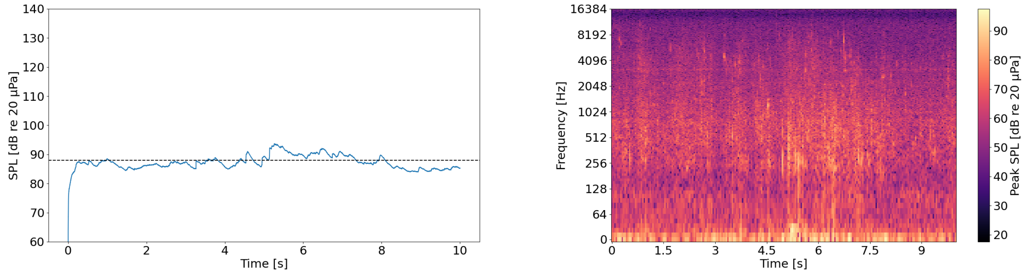

(a) SPL **(b)** Spectrogram

Figure 2.14: Recording of the test subject jumping into the water 11.6 m from hydrophone 2.

The last two examples are from a jump at distances of 5 m and 7.6 m from the hydrophones. These distances are relatively close with similar results, as evident from the plots in Fig. 2.15 and 2.16.

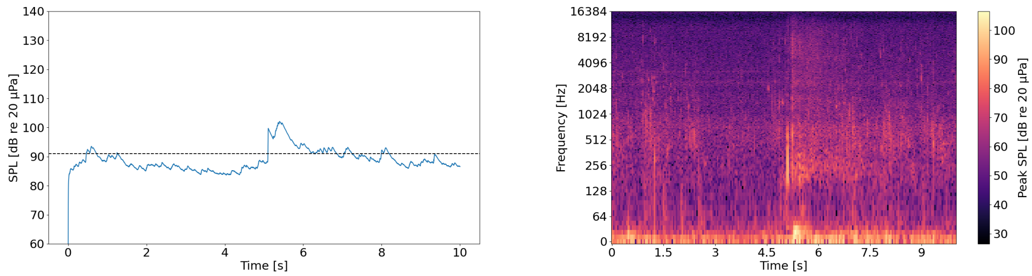

(a) SPL **(b)** Spectrogram

Figure 2.15: Recording of the test subject jumping into the water 5 m from hydrophone 1.

The SPL measurements show matching peaks well above 100 dB and the spectrograms exhibit similar characteristics at the time of the jump. However, the background noise before and after the jump appears to be different, both based on the plots and by listening.

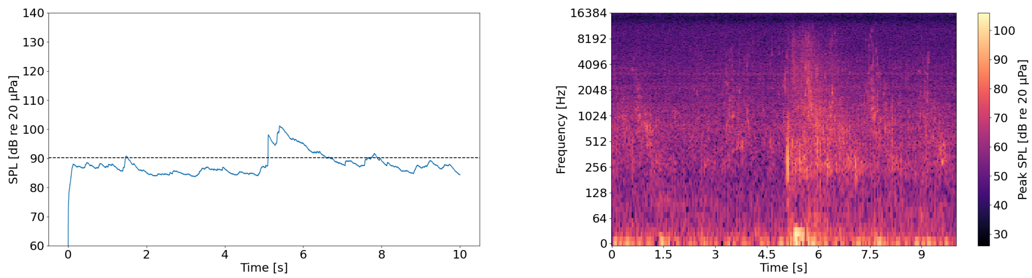

(a) SPL **(b)** Spectrogram

Figure 2.16: Recording of the test subject jumping into the water 7.6 m hydrophone 2.

Although this is not an exhaustive representation of individuals falling into the water, it does provide insight into general spectral tendencies and signal levels.

In general, the signal-to-noise ratio (SNR) appears to be decent without any prominent noise sources. Based on the presented measurements, the signal is expected to be detectable at relatively short distances. A person falling into the water at distances beyond 10 m may still be detectable, but this ultimately relies on the detection algorithm.

The dynamic range within these measurements spans from 70 dB SPL (measured in the evening in Aarhus) up to nearly 130 dB SPL. The desired signal ranges from a few decibels above the background noise, around 80 to 90 dB SPL, up to just below 120 dB SPL, all measured in Aalborg. Furthermore, the frequency range below a few kilohertz appears to be prevalent based on the spectrograms.

2.1.4 Placement of Hydrophones

All field measurements conducted in the analysis were performed with the hydrophones mounted on existing rescue ladders or suspended from the edge of the harbours. The use of rescue ladders facilitated convenient mounting, taking into account the numerous ladders available in both Aalborg and Aarhus. Figure 2.17 provides visual examples of two rescue ladders.

(a) TrygFonden **(b)** Unknown

Figure 2.17: Examples of rescue ladders mounted along the harbour in Aarhus.

The concept of utilising the rescue ladders for hydrophone mounting holds significant potential for a final system, primarily due to their wide availability. It is recommended by TrygFonden to maintain a maximum spacing of 50 m between the ladders, with a preferred spacing of 30 m [19]. Furthermore, the rescue ladders featured in Fig. 2.18 are equipped with solar panels and automatic lighting. These solar panels present a promising opportunity for powering the acoustic detection system.

(a) TrygFonden **(b)** Unknown

Figure 2.18: Solar panels and light on rescue ladders.

Alternatively, the hydrophones could be mounted on buoys or similar objects further out in the water; however, this approach has not been explored. A long-term solution would also require considerations regarding the presence of organic materials, such as those seen growing on the rescue ladders.

2.2 System Requirements

The primary functionality of the system is to detect and locate a person falling into the water and transmit this information to the local emergency services. Once set up and calibrated, the system should operate as a fully automatic stand-alone system. It comprises of two or more underwater sensors, i.e. hydrophones, which are connected to a black box. The black box is responsible for sending a warning signal when a person is suspected to be drowning. A visual overview of this functionality is depicted in the sketch in Fig. 2.19.

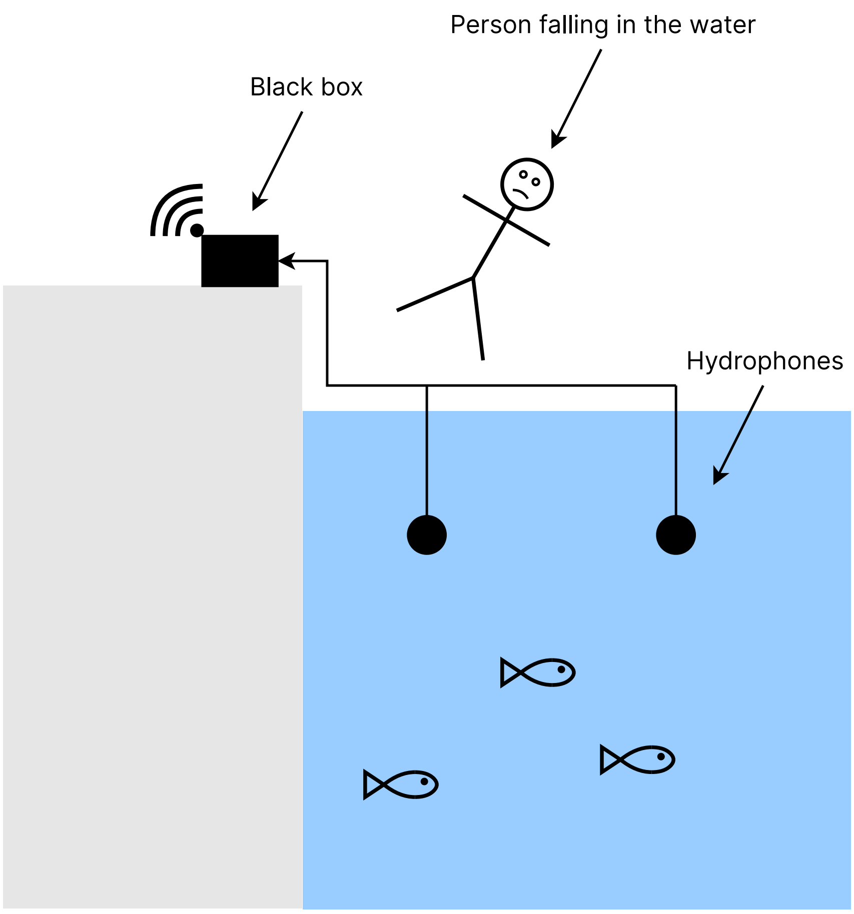

Figure 2.19: Sketch illustrating the functionality of the system.

A set of non-functional requirements is proposed based on the problem analysis in Sec. 1.2 and the field analysis in Sec. 2.1. The requirements are prioritised using the MoSCoW method; dividing these into must (critical), should (important), could (desirable) and won't (unlikely).

Requirements regarding the underwater environmental conditions for the hydrophones:

1. The hydrophones *must* operate within a temperature range of 0 to 30 °C.
2. The hydrophones *must* function in water with a salinity up to 40 ‰.
3. The hydrophones *should* be positioned at a minimum depth of 1 m below the surface.
4. The hydrophones *should* be able to function with depths up to 20 m.

Requirements for the system's acoustical detection capabilities:

5. The system *must* be capable of detecting a person falling into the water at distances up to 5 m from a hydrophone.

6. The system *should* be able to detect a person falling into the water at distances up to 10 m from a hydrophone.

7. The system *could* potentially detect a person falling into the water at distances greater than 10 m from a hydrophone.

8. The system *won't* be designed to detect a person moving around in the water.

Requirements for the operation of the system:

9. The system *must* be battery-powered.

10. The system *should* have the ability to be charged by solar panels.

11. The system *could* be mounted on existing rescue ladders.

Additional regulative requirements:

According to Danish laws § 263 [20], recording conversations in public space is not allowed. Even with low theoretical sound transmission from air to water, this issue should be considered when designing the system. However, it is not considered a formal requirement as there might be legal ways to avoid it, especially if the system is owned and operated by the local authorities.

2.3 Project Delimitation

As outlined in the problem statement in Sec. 1.3, the objective of this project is to investigate the feasibility of utilising affordable custom hydrophones for the detection and localisation of individuals falling into the water. Consequently, the scope of this project is limited to the development of custom hydrophones and the assessment of their usability in a system for warning of drowning accidents in harbours. Furthermore, this project presents considerations regarding the detection algorithm, including the proposed flow and suitable methodologies. The prototype hydrophones developed for the system will serve exclusively as a proof-of-concept to address the formulated research question.

3 System Prototype

This chapter presents the development of the system prototype, encompassing the design and implementation of custom hydrophones as well as considerations regarding the creation of a sophisticated detection algorithm.

3.1 Hydrophone Development

The hydrophones must have a sufficiently high sensitivity to ensure that the acquired signals are significantly above their self-noise and the inherent noise introduced by other equipment in the signal chain. In order to enable effective acoustic detection, it is necessary to cover the entire frequency range of the desired signal, imposing specific requirements on the transducers. Additionally, analogue signal conditioning techniques could be implemented to reduce the noise outside the specific bandwidth of interest, further improving the performance of the system.

Transducers can be omnidirectional or designed with increased sensitivity in specific directions, such as bi-/uni-directional or more complex patterns. By focusing the sound pickup in specific directions, ambient noise levels can be reduced depending on the expected relative positions of the desired signal. Ultimately, the choice of directivity also depends on the final placement and algorithm.

Two different hydrophone prototypes, using inexpensive transducers and custom electronics, are developed for this project, and a picture showcasing the final results can be seen in Fig. 3.1.

Figure 3.1: Custom hydrophone prototypes developed in this project (blue is electret and green is piezoelectric).

The transducers, electronics and mechanics are explained in further detail in the following sections ending with an evaluation of the performance.

3.1.1 Transducers

The most commonly used material for underwater sound transduction is piezoelectric ceramic. However, electrostrictive and magnetostrictive materials are also suitable for this purpose. These three materials are superior for underwater sound, primarily due to their characteristic impedance. However, historically speaking, other transducers such as electrostatic, variable reluctance (electromagnetic), and moving coil (electrodynamic) have been used. It is important to note that this is based primarily on high-power projectors and is not commonly applicable for underwater applications [21].

The spectrum utilised for underwater sound ranges from approximately 1 Hz to beyond 1 MHz [21]. Based on the field analysis in Sec. 2.1, the critical frequency content lies within the range below a few kilohertz. Therefore, most general considerations outlined in the literature regarding underwater transducers can be disregarded. Since no indications towards a specific directivity have been provided, the natural directivity of the transducers is employed.

Most commercial hydrophones (e.g. Brüel & Kjær Type 8104 [22]), as well as do it yourself (DIY) creations (e.g. [9] and [23]), utilise the aforementioned piezoelectric ceramic materials. Given this and the availability of inexpensive piezoelectric transducers in the university laboratory's component stock, it is selected as the primary transducer. Another example of transducers used in DIY hydrophone constructions (e.g. [24]) is the pre-polarised electrostatic microphone. Likewise inexpensive and readily available in the component stock, the electret microphone is chosen as the secondary transducer. Further details on both transducer types are provided in the following sections.

Piezoelectric

Piezoelectricity was discovered in quartz and other crystals by Jacques and Pierre Curie back in 1880. In short, mechanical stress induces an electrical charge, and conversely, an applied electric field causes deformation in the material. This property makes piezoelectric materials excellent for electroacoustic transducers. Additionally, lead zirconate titanate (PZT), a common piezoelectric ceramic material, has a characteristic impedance of 22×10^6 Pa s/m, which is relatively close to that of water (1.5×10^6 Pa s/m) [21].

With minimal loss due to decent impedance matching, piezoceramic transducers appear to be ideal for the application. However, they do have certain drawbacks. Piezoceramic transducers come in various shapes and sizes, such as discs, tubes, films, and bars, and they all have a resonance frequency with an upper limiting roll-off. This resonance frequency can range from a few kilohertz to the megahertz range [25].

For the frequency range of interest, the larger disc [26] shown in Fig. 3.2a is considered sufficient, with a resonant frequency of 4.2 kHz ±500 Hz, while the smaller element [27] has a resonant frequency of 9.5 kHz ±1000 Hz. The relatively low resonant frequency of these elements can be attributed to their primary use as a sound source, such as a buzzer. Nonetheless, these transducers are inexpensive and readily available as off-the-shelf components.

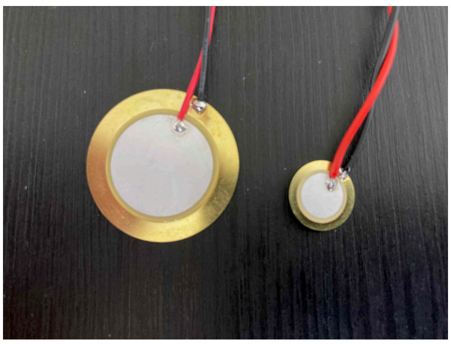

(a) Piezoceremic discs

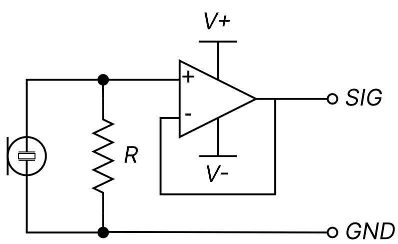

(b) Circuit for interfacing piezoelectric transducers

Figure 3.2: Piezoelectric transducers and interfacing circuitry.

Another issue is the susceptibility of the piezoelectric transducer and its associated cable to electromagnetic interference (EMI). This high sensitivity posed challenges during laboratory measurements, particularly when dealing with the 50 Hz power frequency noise and its harmonics. These interference sources can complicate calibrations and introduce additional noise into the measurements. In certain instances, such as when in close proximity to a power strip, the induced noise can exceed the calibration signal.

The last issue addressed here is the capacitance of the transducer, which requires a high-impedance input to capture low frequencies. For instance, when using the B&K Type 8104 hydrophone with a capacitance of 7.8 nF, a line level input of 10 kΩ results in a low cutoff frequency of 2 kHz. However, when using an instrument input of 1.5 MΩ, the high-pass cutoff is lowered to 14 Hz.

One approach to address this issue is by employing an impedance converter, which can be implemented in various ways. As an example, a circuit using an operational amplifier as an impedance buffer is shown in Fig. 3.2b. With the large piezoceramic disc chosen for the prototype, a 1 MΩ input resistance results in an appropriate lower cutoff frequency of approximately 8 Hz considering its rated capacitance of 20 nF.

Electrostatic

The capacitor-based electret microphone features a diaphragm made of polarised material. This eliminates the need for a polarising voltage source that is typically required by conventional condenser microphones. Behind the dielectric membrane, there is a parallel rigid plate, and the displacement of the membrane relative to the back plate, caused by factors such as sound pressure, generates voltage. This type of transducer is employed in various applications, ranging from inexpensive small devices like the one used in this project (refer to Fig. 3.3a) to high-fidelity recording equipment, such as measurement microphones [17].

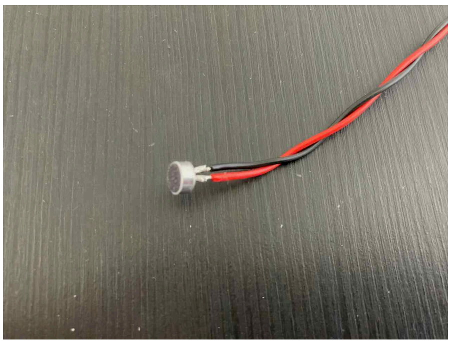

(a) Electret microphone

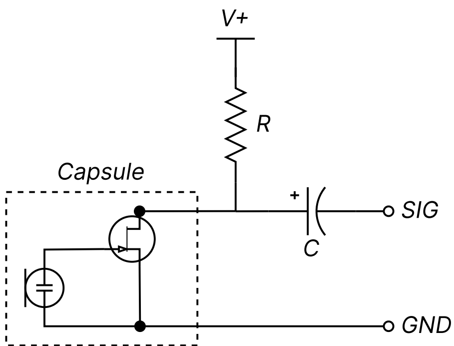

(b) Circuit for interfacing electret microphones

Figure 3.3: Electret microphone and interfacing circuitry.

Inside the capsule of the selected electret microphone [28], there is a field-effect transistor (FET). The FET is utilised as an impedance converter, which necessitates additional circuitry for operation. The interfacing circuit comprises a direct current (DC) voltage source, drain resistor, and a DC-blocking coupling capacitor as seen in Fig. 3.3b.

The typical frequency response of the microphone is provided in the datasheet, indicating a flat response from 20 Hz to 7 kHz. Beyond 7 kHz, the response gradually increases, reaching its peak around +4 dB at 12 kHz, before eventually rolling off at 20 kHz. It's important to note that this frequency response is specified for operation in air, and its performance underwater is unknown.

3.1.2 Electronics

As mentioned, both the piezoelectric and electret transducers require additional electronic circuits for proper functioning. Placing the electronics close to the single-ended (unbalanced) transducer output allows for a conversion to differential (balanced) signalling, which provides a better noise reduction. Another reason for placing the electronics near the transducer is to minimise the noise experienced when handling the cables of the reference hydrophones as described in Appx. B. Furthermore, a shielded twisted pair cable is used from the circuit to the XLR connector to improve the signal-to-noise ratio (SNR) [29].

From a practical standpoint, as mentioned in the system requirements in Sec. 2.2, the electronics in a final system should be battery-powered and ideally capable of being charged by solar panels, such as the ones available on the rescue ladders. However, this prototype is designed to be powered by phantom power, and the circuit design takes inspiration from [9].

The schematic provided in Fig. 3.4 illustrates the impedance buffer circuit for the piezoceramic transducer and the conversion from single-ended to differential signalling. When viewed from the transducer side, the circuit provides an input resistance of 1 MΩ and routes the signal through a non-inverting and inverting buffer to generate the differential signal. The TLC272 dual operational amplifier is selected for its low input bias current of less than 60 pA, which is crucial considering the large input resistor. Furthermore, the TLC272 boasts a low supply current of under 3.6 mA, a necessary feature as the circuit is powered by P48 phantom power, conforming to the maximum current of 10 mA specified in the DS/EN IEC 61938 standard [30].

Phantom power is supplied through two 2.2 kΩ resistors and regulated down to 12 V using a zener diode. The voltage supply is then stabilised with a 47 µF capacitor. To filter out any potential noise from the zener diode, a low-pass filter is implemented at 17 Hz, consisting of a 200 Ω resistor and a 47 µF capacitor. A virtual ground reference is established using two 47 kΩ resistors and stabilised with a 47 µF capacitor. Finally, the output from the operational amplifiers is coupled to the phantom power through two 47 Ω resistors, and high-frequency decoupling is achieved using two 0.1 µF capacitors.

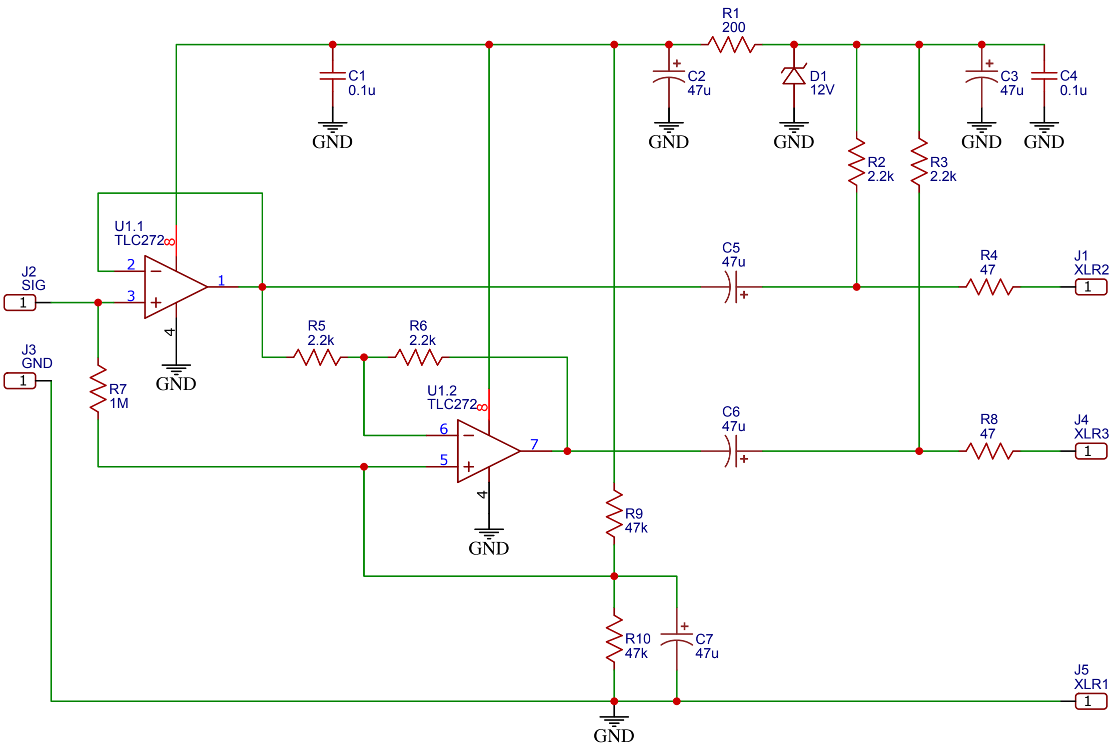

Figure 3.4: Schematic of impedance buffer circuit for the piezoceramic transducer.

The circuit for the electret transducer, shown in Fig. 3.5, shares similarities with the piezoelectric transducer circuit. However, it features a lower input resistance of 47 kΩ and includes an auxiliary circuit for driving the electret microphone. The additional circuit is powered through a 6.8 kΩ resistor and regulated down from 12 V to 5 V using another zener diode.

The voltage supply is stabilised and decoupled using 47 µF and 0.1 µF capacitors. The recommended 2.2 kΩ gain resister is employed and a 4.7 µF coupling capacitor blocks the DC supply below 1 Hz. Furthermore, this circuit incorporates another operational amplifier, the OP275, which offers improved noise performance with a rating of 6 nV/$\sqrt{\text{Hz}}$ compared to the TLC272's 25 nV/$\sqrt{\text{Hz}}$ (both specified at 1 kHz).

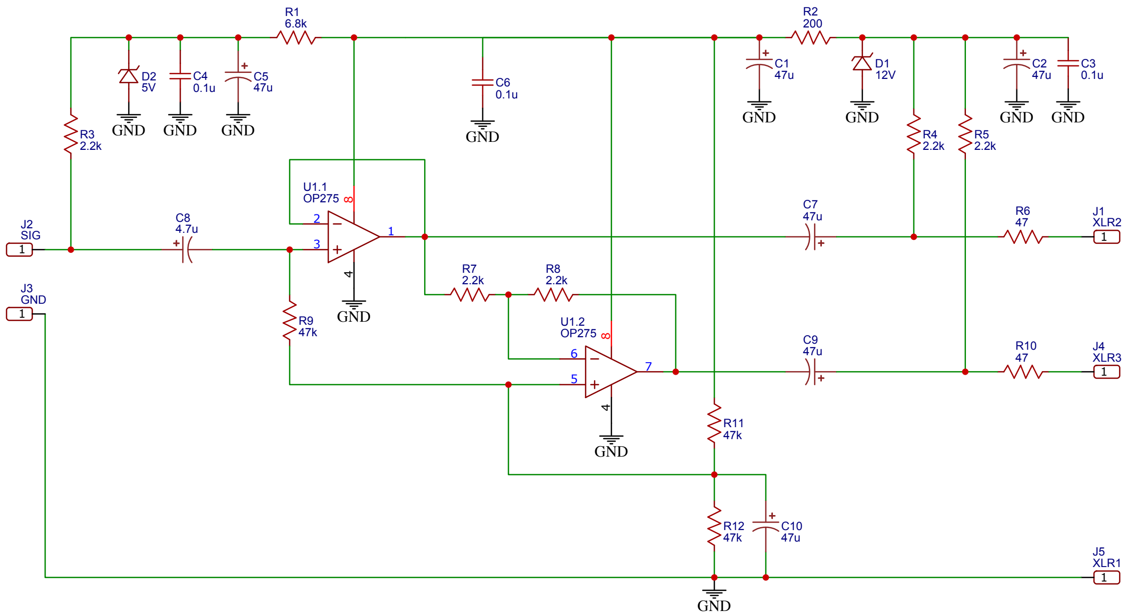

Figure 3.5: Schematic of impedance buffer circuit for the electret transducer.

Both the circuit diagrams and soldering layouts were created using the online printed circuit board (PCB) design tool EasyEDA [31]. The two layouts have a high degree of similarity, as seen in Fig. 3.6.

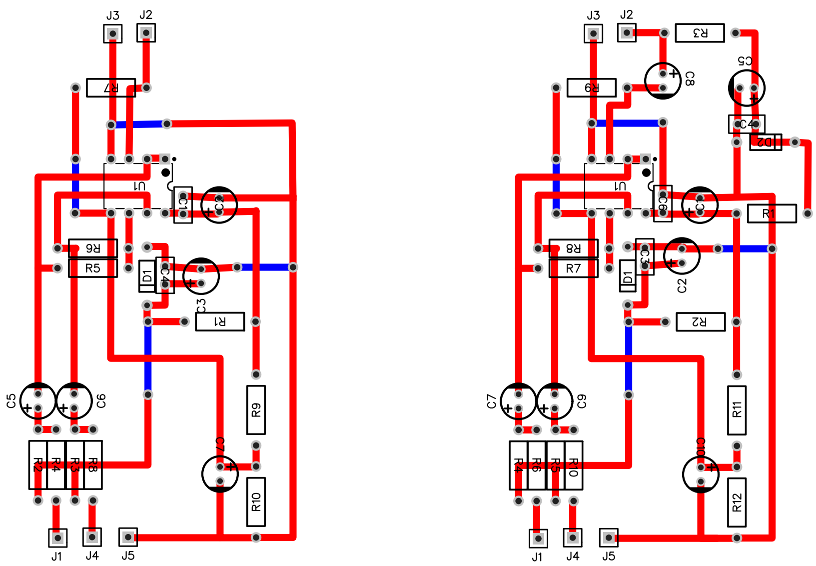

(a) Piezoceremic transducer

(b) Electret transducer

Figure 3.6: Soldering layouts for the two custom hydrophones (red = wires and blue = jumpers).

Based on the soldering layout, the two hydrophone prototypes are assembled on a stripboard, as shown in Fig. 3.7.

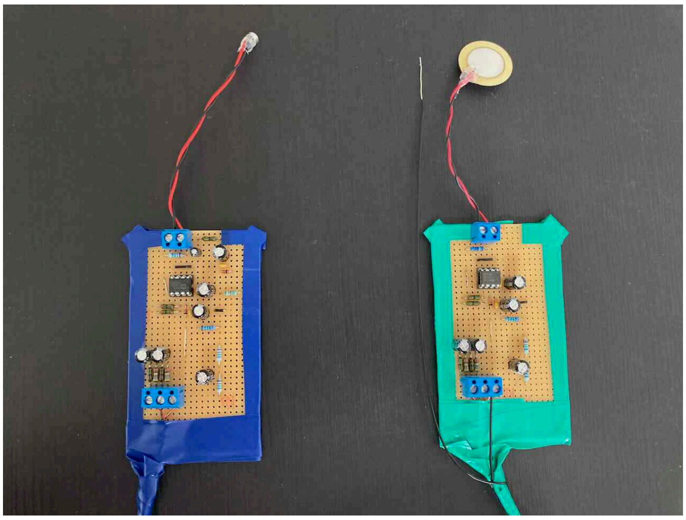

Figure 3.7: Custom hydrophones including electronics assembled on the stripboards (blue is electret and green is piezoelectric).

Twisted pair cabling is utilised from each transducer to the board, and screw-on terminals are implemented for easy switching. Additionally, a ground wire (seen as the black wire to the left of the green hydrophone in Fig. 3.7) is added to establish a common ground reference with the water for the piezoelectric transducer. This connection helps mitigate the interference caused by power frequency noise, predominant when the hydrophone is submerged in water.

3.1.3 Mechanics

The outer layer of a hydrophone must be waterproof to protect the electronic circuit and connections from the conductive nature of water. It is desirable for the material to be acoustically transparent, and achieving impedance matching with water is crucial for optimal sound transmission through this decoupler [21].

There are several approaches to achieving this. For example, the B&K Type 8104 hydrophone is moulded using nitrile butadiene rubber, while other moulds, as done in [9], utilise urethane resin. Both options provide satisfactory solutions with effective protection and acoustic transparency. However, during the prototyping phase, moulding is not the most ideal solution. It is advantageous to have the flexibility to make changes to both the electronics and transducers through iterations and ongoing testing. In this case, nitrile rubber gloves, commonly available in most grocery stores, are used to embed the electronics and transducers, as depicted in Fig. 3.8.

Figure 3.8: Custom hydrophones embedded in nitrile rubber gloves (blue is electret and green is piezo-electric).

Even with careful stretching of the rubber around the transducer, air can still be trapped, particularly in the capsule of the electret transducer. One potential solution to minimise the lossy water-to-air transmission is to fill the air volume surrounding the membrane with oil, as demonstrated in [24]. However, it is important to note that this approach has not been tested.

3.1.4 Evaluation

There are international standards for underwater acoustics including hydrophone calibration. While this level of accuracy is evaluated unnecessarily for the project in particular, a brief introduction to the approaches is provided. This is followed by a description of the actual method used and the obtained results. More detailed information about the setup and results can be found in Appx. A.3.

Standardised Methods

DS/EN IEC 60565 Part 1 [32], outlines the "Free-field calibration by comparison with an acoustic reference device." This procedure is conducted under free-field conditions, typically requiring a large water tank, and covers the frequency range from 200 Hz to 1 MHz. The second part of the standard addresses "Procedures for low-frequency pressure calibration" and is described in DS/EN IEC 60565 Part 2 [33]. Depending on the method used, this part covers frequencies from 0.01 Hz to 5 kHz.

One of the methods described in the second part involves calibration by pistonphone, but unfortunately a hydrophone calibrator was not available at the laboratory. Instead, custom three-dimensional (3D)-printed couplers were used together with a standard pistonphone for calibration of the reference hydrophones, as described in Appx. A.2.

A technical review by Brüel & Kjær [34] presents a method for air calibration in an anechoic chamber, valid in the frequency range of 50 Hz to 4 kHz, where diffraction phenomena can be neglected. This method relies on the hydrophone having a sufficiently high acoustical impedance to disregard its radiation impedance. However, such calibration method has not been explored in this project, as measurements of the actual acoustic impedance of the custom hydrophones have not been conducted to verify its applicability.

Chosen Method

A customised measurement setup is constructed to calibrate the custom hydrophones and compare their frequency responses. Instead of allocating resources to absolute calibration, a bucket filled with water is used for relative measurements, referencing the calibration standard hydrophone B&K Type 8104.

While the B&K hydrophone can also be used for sound projection, its frequency response exhibits a peak sensitivity of around 111 dB re 20 μPa/V at 90 kHz with a 12 dB/octave slope [22]. Consequently, its low-frequency output, which is of particular interest, is relatively poor. To address this, low-frequency measurements were conducted using an audio exciter mounted on the end of the bucket, as depicted in Fig. 3.9.

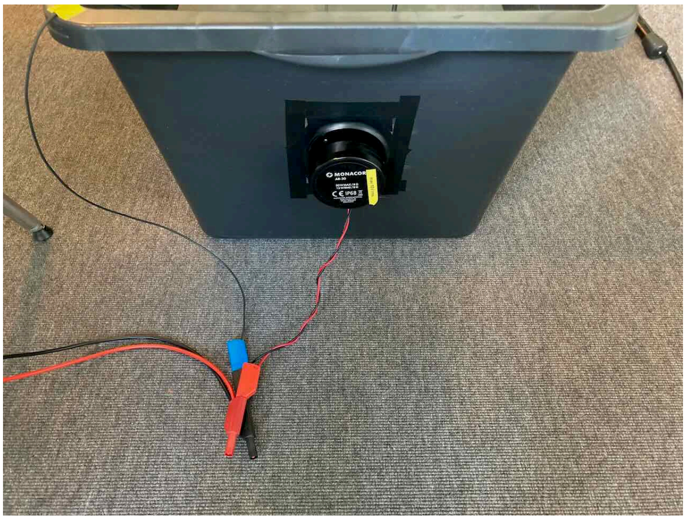

Figure 3.9: Audio exciter mounted on the end of the mortar bucket.

Assuming the water-filled mortar bucket is a closed rectangular cavity, the highest acoustic pressure occurs at the junction of three surfaces [17]. This maximum pressure is a result of the pressure anti-node of low-frequency modes. To minimise the influence of spatial variations, the hydrophone is positioned in the lower corner of the bucket. Reference measurements are conducted with the hydrophone placed opposite the sound source, as depicted in Fig. 3.10.

(a) Top-view

(b) Close-up

Figure 3.10: Reference hydrophone placed in the corner of the mortar bucket.

The custom hydrophones are calibrated using a substitution procedure, where they consecutively are placed in the same position as the reference hydrophone (see Fig. 3.11) while the same sound field is generated.

(a) Piezoelectric **(b)** Electret

Figure 3.11: Custom hydrophones placed in the corner of the mortar bucket.

The 90 L mortar bucket has its largest dimensions of 80 cm × 50 cm × 31.5 cm, and with a speed of sound in freshwater of 1481 m/s at 20 °C, the lowest normal mode occurs at 925.6 Hz. This frequency is reached when the wavelength is equal to two times the largest dimension of the bucket and is calculated by

$$f_m = \frac{c}{2l} \tag{3.1}$$

where

f_m	=	frequency of axial mode	[1/s]
c	=	speed of sound	[m/s]
l	=	largest dimension	[m]

Below this frequency, the bucket behaves primarily as a pressure field with little to no spatial variations. Above this frequency, the modal variations are reduced by positioning the transducers in the corner of the bucket.

Results

The sensitivity of all hydrophones is calibrated to 112 dB re 20 µPa at 250 Hz, and their relative frequency responses are measured using sine sweeps. While the specific directivity pattern has not been determined, each measurement is repeated to assess variability. The frequency responses of all hydrophones, obtained from a single measurement for each, are presented in Fig. 3.12.

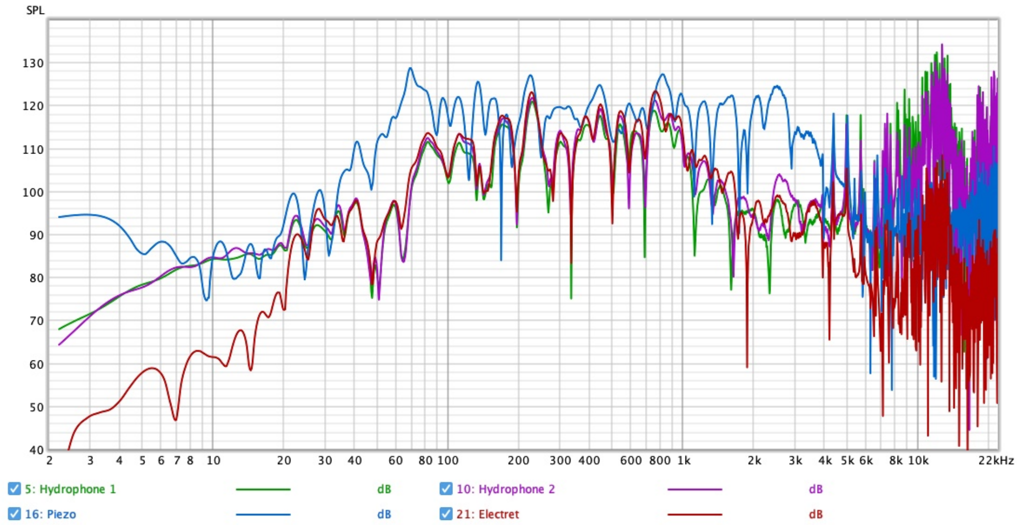

Figure 3.12: Frequency response of all hydrophones.

As observed in the plot, there are multiple peaks and dips in the frequency responses. The electret hydrophones closely track the response of the reference hydrophones, while the piezoelectric hydrophone exhibits some deviation. Additionally, the calibration at 250 Hz occurs on a slope between a peak and a dip, resulting in a misalignment of the frequency responses that complicates visual comparison. To address this, third-octave smoothed and aligned frequency responses are presented in Fig. 3.13. The misalignment is corrected by averaging over two octaves centred at 250 Hz.

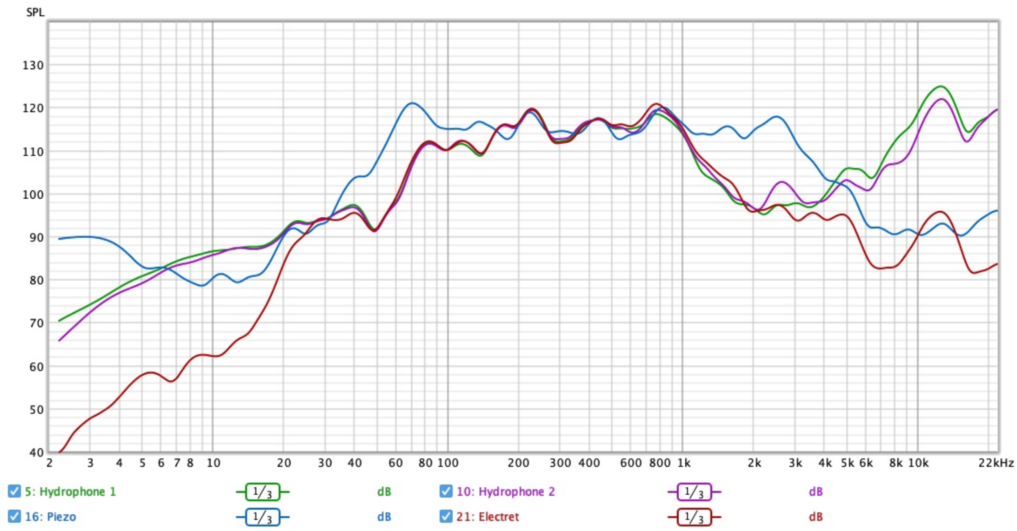

Figure 3.13: Frequency response of all hydrophones (1/3 octave smoothing and aligned).

From this plot, it is evident that the frequency response of the electret hydrophone closely matches the reference hydrophones from just over 20 Hz up to at least 2 kHz. A gradual decrease in sensitivity at low frequencies is expected since the manufacturer only claims its response to be flat down to 20 Hz in air. At higher frequencies, the physical construction of the hydrophone starts to affect the sound field, leading to deviations. Additionally, the water-to-air transmission might also affect the high frequency response.

On the other hand, the piezoelectric hydrophone does not exhibit a low-frequency roll-off. However, its relative sensitivity is higher than the reference hydrophones in the frequency ranges of approximately 30 to 250 Hz and 1 to 4 kHz. It is important to note that the SNR also deteriorates at low frequencies for all hydrophones, which can impact the validity of the results.

Examining the background noise measurements presented in Fig. 3.14, distinct variations can be observed among the hydrophones under test. All hydrophones are affected by the 50 Hz power frequency noise and its harmonics. However, the piezoelectric hydrophone exhibits by far the worst noise performance. In contrast, the electret hydrophone demonstrates even lower noise levels than the references. It should be noted that the difference between instrument and microphone inputs might also affect these results.

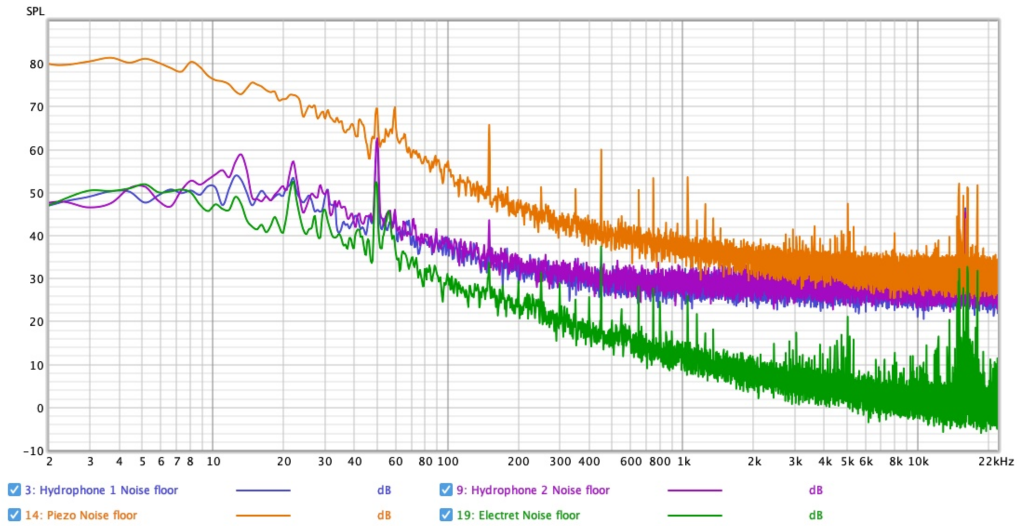

Figure 3.14: Noise floor spectra with all hydrophones.

The piezoelectric hydrophone exhibits a higher full band noise floor of 91 dB sound pressure level (SPL) compared to the reference hydrophones, which were measured at 73 dB and 74 dB, and the electret at 63 dB. Considering the findings from the field analysis in Sec. 2.1, this elevated noise level could pose challenges for the piezoelectric hydrophone. However, there is potential for improvement by enhancing the electronics and employing digital signal processing (DSP) techniques.

Evaluation of the frequency responses reveals promising performance for both the piezoelectric and electret transducers. Nevertheless, when examining the spectrograms of the desired signals in the field analysis, the low-frequency roll-off of the electret hydrophone may have a negative impact on its performance. This consideration is highly dependent on the detection algorithm.

3.2 Algorithm Considerations

As introduced in the problem analysis in Sec. 1.2 and specified in the system requirements in Sec. 2.2, the proposed signal detection task involves both recognition and localisation of the underwater acoustic event. From a high-level perspective, the process begins with retrieving a new audio buffer containing recorded underwater sound.

The initial task is to determine whether an acoustic event is present in the buffered audio. If an event is detected, the algorithm then classifies it as either a person falling into the water or noise. Finally, if the acoustic event is recognised as a person, the algorithm aims to localise the position of this sound source. The flow of this algorithm is visualised in Fig. 3.15.

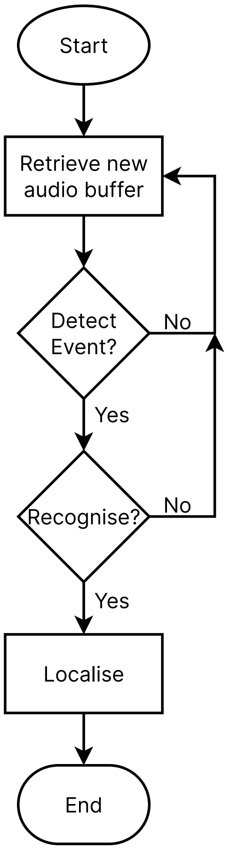

Figure 3.15: Flow diagram of the proposed algorithm.

Developing an algorithm for the aforementioned task is a complex endeavour and not the primary focus of this project. However, it is an integral part of the final system, and initial reflections have been made alongside the analysis and development process. Developing a well-functioning algorithm necessitates a diverse data set, and thereby extensive data collection, which has not been carried out in this project.

The actual deployment of the algorithm could be challenging due to the variability of environmental conditions, background noise, and the inherent limitations of the sensors. Thorough field testing would be essential to validate the algorithm's performance in real-world scenarios, followed by appropriate refinement to enhance its effectiveness.

Despite the aforementioned limitations, the subsequent sections will outline some of the potential methods and techniques that could have been employed for algorithm development.

3.2.1 Event Detection

There are many types of intelligent systems, which here will be categorised into three types: classic DSP, traditional machine learning (ML) and deep learning (DL). In this context, the event detection and recognition tasks are separated to enable the implementation of a low-processing DSP algorithm that operates in real-time, thereby optimising power consumption. If the detection task performs adequately, it may obviate the need for more resource-intensive ML methods.

To enhance the audio signals and mitigate noise, appropriate pre-processing techniques should be employed. These techniques can range from simple band-limiting filters to more advanced noise-reduction methods. The specific data-cleaning approach should be based on the performed analysis and employ general heuristics.

Event detection can be accomplished through various approaches, but a simple yet effective method involves observing the sound pressure level. A high SPL indicates a deviation from the background noise, potentially indicating the presence of an event. The field analysis reveals that several sources can generate high amplitudes; however, notable differences emerge in the temporal scope. By employing a sliding window technique, impulsive events can be identified while minimising false detection. For instance, this approach might detect impulsive noises like breaking waves or objects being dropped into the water, while potentially disregarding most vessel-related sounds.

Such an algorithm would rely on a set of handcrafted rules to determine if an acoustic event has occurred. Subsequently, the recognition task involves classifying the sounds and determining whether they correspond to a person falling into the water or some other event.

3.2.2 Recognition

Recognising patterns and classifying data are fundamental tasks in machine learning, where extracting relevant features from raw audio signals aids in discriminating between different acoustic events. Typical audio features used in classical ML for speech and music discrimination include temporal (e.g., zero-crossing rate, energy) and spectral (e.g., spectral centroid, spectral flux, mel-frequency cepstral coefficients (MFCCs)), combined with statistical measures (e.g., mean, variance) [35].

The selection of optimal features requires domain knowledge and is often referred to as feature engineering. In this specific case, valuable insights can be derived from the theoretical and practical analysis. Particularly the identified low-frequency impulsive sounds could serve as a baseline.

Deep learning has witnessed significant advancements in recent years, offering a data-driven approach that differs from classical methods. Instead of manually selecting features, deep learning (DL) models leverage unstructured data, allowing multiple neural network layers to perform automatic feature extraction. This can either be done from the raw audio waveform in the time domain or some form of time-frequency spectrograms (e.g., log-frequency, log-mel, constant-Q). The latter approach is commonly used in conjunction with image classification methods such as convolutional neural networks (CNNs) [36].

One idea is to employ supervised learning, where the model is trained on labelled data, necessitating a substantial amount of high-quality recordings of acoustic events. If processing resources and power consumption are not major concerns or due to recent technological advancements, event detection and recognition can be combined into a single real-time task. Nevertheless, a diverse collection of underwater recordings encompassing instances of people falling into the water, ambient underwater sounds, and other background noises would still be necessary.

An alternative approach is anomaly detection, also known as outlier detection or novelty detection, which aims to identify data instances that significantly deviate from the majority of instances [37]. Collecting sufficient and representative data could be time-consuming and challenging, given the rarity of people falling into the water compared to normal acoustic events in a harbour. Instead, a model could be trained on all other sounds that can be easily recorded without direct oversight, leading to the detection of the anomaly represented by people falling into the harbour.

3.2.3 Localisation

Once an acoustic event is detected and recognised as a person falling into the water, determining their location becomes crucial for providing valuable information to emergency services. Accuracy requirements for location determination are not specified since this is highly dependent on geographical aspects. For example, in areas with strong currents like Limfjorden, a person may be displaced significantly compared to a harbour basin with minimal or no flow.

If it is assumed that a person stays close to the point of initial contact with the water, the location could simply be determined by identifying the closest sensor. This can be achieved by analysing the relative level difference of the impact sound. The hydrophone detecting the loudest signal would also be the closest, and the location could be further refined by considering a weighting between the two closest hydrophones to estimate a midpoint.

Alternatively, triangulation techniques could be used by examining the relative time difference of arrival (TDOA) between adjacent sensors. This approach has the potential to provide higher resolution compared to using the relative level difference.

Expanding the system to utilise multiple hydrophones, forming a sensor array, opens up possibilities for both simple and more advanced beamforming techniques (e.g. spectral-based, parametric). These techniques can estimate the direction of arrival (DOA) and time delay from a reference point, enhancing the accuracy of location estimation [38]. Furthermore, deep learning methods can also be explored for sound source localisation using multiple microphones and leveraging the additional information available from spatial sampling [36].

4 Conclusion

In summary, this project has provided valuable insights into underwater acoustics in harbours and the potential use of hydrophones for detecting a person falling into the water. Based on careful analysis of the problem and on-site measurements, prototypes of custom and inexpensive hydrophones were developed and compared to calibrated reference hydrophones.

Evaluation of the custom hydrophones yielded promising results for both the piezoelectric and electret transducers, highlighting their suitability as key components in an acoustic detection system. However, certain issues, such as high inherent noise levels from the piezoelectric hydrophone and a low-frequency roll-off of the electret, were identified, suggesting further investigation to understand their impact on system-level performance.

This project has successfully provided hydrophone prototypes and suggestions for inexpensive transducers, laying the foundation for further optimisations. For instance, exploring technologies like microelectromechanical systems (MEMS) and surface-mount devices (SMDs) on printed circuit boards (PCBs) could significantly reduce the physical size of the hydrophones, enhancing their practicality and deployment feasibility.

To fully realise a functioning system, the proposed algorithm must be developed. Various methods for recognition and localisation seem viable, and expanding the algorithm to detect a person's movements within the water, beyond the initial splash, could enhance its usability. This novel approach to preventing drowning accidents could be integrated effectively with existing safety infrastructure and potentially save lives. Nevertheless, human intervention is crucial to validate warning signals and coordinate rescue tasks, putting pressure on the available resources.

While it has been argued that even thermal cameras would not have prevented the recent drowning accident in Aalborg [39], a broad effort is necessary to provide a reliable lifesaving solution. This might include increasing awareness and implementing supplementary physical initiatives, such as lighting and fencing. Thus, it is important to acknowledge its limitations and the need for scientific validation of the effectiveness of these preventive measures.

Additionally, exploring the concept of a ”smart ocean”, using underwater acoustic communication between various sensors, presents intriguing opportunities. However, challenges may arise if the Internet of Underwater Things (IoUT) [40] utilises interfering frequencies. Moreover, the usage of inexpensive hydrophones and acoustic detection could be extended to other scenarios such as streams, and swimming pools as well as for surveillance activities.

In conclusion, this study demonstrates the viability of using inexpensive custom hydrophones in an acoustic detection system to prevent drowning accidents in harbours. Incorporating these findings into the development of an actual system could contribute to saving lives and creating safer harbour environments.

Acronyms

3D three-dimensional 25, 41, 55

CNN convolutional neural network 31

DC direct current 21

DIY do it yourself 3, 20

DL deep learning 30

DOA direction of arrival 32

DSP digital signal processing 29

EMI electromagnetic interference 21

FET field-effect transistor 21

FFT fast Fourier transform 60

IoUT Internet of Underwater Things 33

MEMS microelectromechanical systems 33

MFCC mel-frequency cepstral coefficient 31

ML machine learning 30

PCB printed circuit board 23, 33

PZT lead zirconate titanate 20

RMS root mean square 44

SMD surface-mount device 33

SNR signal-to-noise ratio 8, 15, 22

SONAR sound navigation and ranging 3

SPL sound pressure level 9, 29, 50, 60

TDOA time difference of arrival 32

Bibliography

[1] Rådet for Større Bade- og Vandsikkerhed. 'Druknedøde i danmark 2021,' badesikkerhed.dk. (5th Apr. 2022), [Online]. Available: https://www.badesikkerhed.dk/druknedoede-i-danmark-2021/ (visited on 22/01/2023).

[2] Ritzau. 'Flere omkommer ved drukneulykker i danske havne,' politiken.dk. (30th Dec. 2022), [Online]. Available: https://politiken.dk/indland/art9146809/Flere-omkommer-ved-drukneulykker-i-danske-havne (visited on 22/01/2023).

[3] Ritzau. 'Organisation om drukneulykker: Man kan gøre meget mere,' politiken.dk. (16th Mar. 2022), [Online]. Available: https://politiken.dk/indland/art8671667/Organisation-om-drukneulykker-Man-kan-g%C3%B8re-meget-mere (visited on 22/01/2023).

[4] B. N. Hald. '0 drukneulykker ved aarhus havn: Ny indsats har virket,' tv2ostjylland.dk. (26th Dec. 2022), [Online]. Available: https://www.tv2ostjylland.dk/artikel/sikker-havn (visited on 22/01/2023).

[5] V. N. Bjerre. 'Antallet af drukneulykker i havne stiger: Men borgmester ikke med på sikkerhedshegn - endnu,' nordjyske.dk. (31st Dec. 2022), [Online]. Available: https://nordjyske.dk/nyheder/aalborg/antallet-af-drukneulykker-i-havne-stiger-men-borgmester-ikke-med-paa-sikkerhedshegn-endnu/4067929 (visited on 22/01/2023).

[6] L. E. Julsgaard. 'Termiske kameraer har reddet to mennesker fra at drukne - her er prisen for at sikre resten af havnefronten,' nordjyske.dk. (23rd Feb. 2022), [Online]. Available: https://nordjyske.dk/nyheder/aalborg/kameraer-har-reddet-to-mennesker-i-aalborg-havn-lige-uden-for-deres-raekkevidde-faldt-oliver-i-vandet/c852956a-a75a-402b-8f3b-6ce0fb8f9abf (visited on 22/01/2023).

[7] R. J. Urick, *Principles of Underwater Sound*, 3rd ed. Peninsula Publishing, 2013.

[8] K. Sørensen, J. Christensen-Dalsgaard and M. Wahlberg, 'Is human underwater hearing mediated by bone conduction?' *Hearing Research*, p. 108 484, Jul. 2022. DOI: 10.1016/j.heares.2022.108484.

[9] DJJules. 'Let's build some world class hydrophones,' instructables.com. (2022), [Online]. Available: https://www.instructables.com/Lets-Build-Some-World-Class-Hydrophones/ (visited on 01/02/2023).

[10] The Danish Environmental Protection Agency. 'Vandområdeplaner - basisanalyser,' mst.dk. (2004), [Online]. Available: https://mst.dk/natur-vand/vandmiljoe/vandomraadeplaner/vandplaner-2009-2015/hoeringer/hoering/basisanalyser/ (visited on 02/03/2023).

[11] sea temperature. 'Water temperature on the world's beaches,' seatemperature.net. (2023), [Online]. Available: https://seatemperature.net (visited on 02/03/2023).

[12] DMI. 'Tidevandstabeller,' dmi.dk. (2023), [Online]. Available: https://www.dmi.dk/hav-og-is/temaforside-tidevand/tidevandstabeller/ (visited on 17/03/2023).

[13] Geological Survey of Denmark and Greenland. 'Seabed sediment map,' eng.geus.dk. (2004), [Online]. Available: https://eng.geus.dk/mineral-resources/danish-raw-materials/seabed-sediment-map (visited on 03/03/2023).

[14] Statistics Denmark. 'Maritime transport over danish ports,' dst.dk. (2021), [Online]. Available: https://www.dst.dk/en/Statistik/dokumentation/documentationofstatistics/maritime-transport-over-danish-ports (visited on 03/03/2023).

[15] Eniro Sverige AB. 'Krak til søs,' tilsos.krak.dk. (2022), [Online]. Available: https://tilsos.krak.dk (visited on 02/03/2023).

[16] Aarhus Kommune. 'Aarhus ø,' aarhusoe.dk. (2023), [Online]. Available: https://aarhusoe.dk (visited on 03/03/2023).
[17] L. E. Kinsler, A. R. Frey, A. B. Coppens and J. V. Sanders, *Fundamentals of Acoustics*, 4th ed. Wiley, 2000.
[18] Audacity. 'Audacity,' audacityteam.org. (2023), [Online]. Available: https://www.audacityteam.org (visited on 19/05/2023).
[19] TrygFonden Kystlivredning. 'Hvordan kan i selv gøre havnen mere sikker?' respektforvand.dk. (2022), [Online]. Available: https://www.respektforvand.dk/viden-og-materialer/redningskrans/ansoeg-om-redningsstige/hvordan-kan-i-selv-goere-havnen-sikker (visited on 13/05/2023).
[20] Retsinformation. '§ 263,' retsinformation.dk. (2021), [Online]. Available: https://www.retsinformation.dk/eli/lta/2021/1851#P263 (visited on 03/02/2023).
[21] J. L. Butler and C. H. Sherman, *Transducers and Arrays for Underwater Sound*. Springer International Publishing, 2016. DOI: 10.1007/978-3-319-39044-4.
[22] Brüel & Kjær. 'Type 8104 calibration standard hydrophone,' bksv.com. (2023), [Online]. Available: https://www.bksv.com/en/transducers/acoustic/microphones/hydrophones/8104 (visited on 01/05/2023).
[23] F. Blume and S. Lana. 'DIY hydrophone,' felixblume.com, [Online]. Available: https://felixblume.com/hydrophone/ (visited on 01/02/2023).
[24] action_owl. 'Underwater microphone (hydrophone),' instructables.com, [Online]. Available: https://www.instructables.com/Underwater-Microphone-Hydrophone/ (visited on 01/02/2023).
[25] APC International, Ltd. 'American piezo ceramics,' americanpiezo.com, [Online]. Available: https://www.americanpiezo.com (visited on 14/05/2023).
[26] RS Components A/S. 'RS PRO piezo buzzer (large),' dk.rs-online.com, [Online]. Available: https://dk.rs-online.com/web/p/piezo-summere/7243162 (visited on 08/05/2023).
[27] RS Components A/S. 'RS PRO piezo buzzer (small),' dk.rs-online.com, [Online]. Available: https://dk.rs-online.com/web/p/piezo-summere/8377844 (visited on 08/05/2023).
[28] RS Components A/S. 'RS PRO 6mm microphone condenser,' dk.rs-online.com, [Online]. Available: https://dk.rs-online.com/web/p/kondensatormikrofon-komponenter/7717011 (visited on 08/05/2023).
[29] H. W. Ott, *Noise Reduction Techniques in Electronic Systems*, 2nd ed. Wiley, 1988.
[30] DS/EN IEC 61938, *Multimedia systems - guide to the recommended characteristics of analogue interfaces to achieve interoperability*, 2018.
[31] EasyEDA. 'EasyEDA,' easyeda.com, [Online]. Available: https://easyeda.com (visited on 10/05/2023).
[32] DS/EN 60565-1, *Underwater acoustics - hydrophones - calibration of hydrophones - part 1: Procedures for free-field calibration of hydrophones*, 2020.
[33] DS/EN 60565-2, *Underwater acoustics - hydrophones - calibration of hydrophones - part 2: Procedures for low frequency pressure calibration*, 2019.
[34] Brüel & Kjær, *Technical review 1973-1 calibration of hydrophones*, 1973.
[35] E. Scheirer and M. Slaney, 'Construction and evaluation of a robust multifeature speech/music discriminator,' in *1997 IEEE International Conference on Acoustics, Speech, and Signal Processing*, 1997, pp. 1331–1334. DOI: 10.1109/ICASSP.1997.596192.
[36] H. Purwins, B. Li, T. Virtanen, J. Schluter, S.-Y. Chang and T. Sainath, 'Deep learning for audio signal processing,' *IEEE Journal of Selected Topics in Signal Processing*, no. 2, pp. 206–219, May 2019. DOI: 10.1109/JSTSP.2019.2908700.
[37] G. Pang, C. Shen, L. Cao and A. V. D. Hengel, 'Deep learning for anomaly detection: A review,' *ACM Computing Surveys*, no. 2, pp. 1–38, Mar. 2022. DOI: 10.1145/3439950.
[38] H. Krim and M. Viberg, 'Two decades of array signal processing research: The parametric approach,' *IEEE Signal Processing Magazine*, no. 4, pp. 67–94, Jun. 1996. DOI: 10.1109/79.526899.
[39] S. Skov. 'Bentes søn oliver druknede i limfjorden: - det må ikke ske for flere,' nordjyske.dk. (29th Jun. 2022), [Online]. Available: https://nordjyske.dk/nyheder/

nordjylland/bentes-soen-oliver-druknede-i-limfjorden-det-maa-ikke-ske-for-flere/3032123 (visited on 22/01/2023).
[40] R. A. Khalil, N. Saeed, M. I. Babar and T. Jan, 'Toward the internet of underwater things: Recent developments and future challenges,' *IEEE Consumer Electronics Magazine*, no. 6, pp. 32–37, 1st Nov. 2021. DOI: 10.1109/MCE.2020.2988441.
[41] DS/ISO/IEC 98-3, *Guide to the expression of uncertainty in measurements*, 2008.
[42] GRAS Sound & Vibration. '26ca 1/2" CCP standard preamplifier with BNC connector,' grasacoustics.com. (2023), [Online]. Available: https://www.grasacoustics.com/products/preamplifiers-for-microphone-cartridge/constant-current-power-ccp/product/203-26ca (visited on 01/05/2023).
[43] GRAS Sound & Vibration. '12aq 2-channel universal power module with signal conditioning and PC interface,' grasacoustics.com. (2023), [Online]. Available: https://www.grasacoustics.com/products/power-module/traditional-power-supply-lemo/product/228-12aq (visited on 01/05/2023).
[44] John Mulcahy. 'Room EQ wizard,' roomeqwizard.com. (2022), [Online]. Available: https://www.roomeqwizard.com (visited on 18/05/2023).
[45] DMI. 'Vejrarkiv,' dmi.dk. (2023), [Online]. Available: https://www.dmi.dk/lokationarkiv/ (visited on 20/03/2023).
[46] Python Software Foundation. 'Python,' python.org. (2023), [Online]. Available: https://www.python.org (visited on 19/05/2023).
[47] NumPy. 'NumPy,' numpy.org. (2023), [Online]. Available: https://numpy.org (visited on 19/05/2023).
[48] The Matplotlib development team. 'Matplotlib,' matplotlib.org. (2023), [Online]. Available: https://matplotlib.org (visited on 19/05/2023).
[49] SciPy. 'SciPy,' scipy.org. (2023), [Online]. Available: https://scipy.org (visited on 19/05/2023).
[50] librosa development team. 'Librosa,' librosa.org. (2023), [Online]. Available: https://librosa.org (visited on 19/05/2023).

Part II

Appendix

A Laboratory Measurements

A.1 Expression of Uncertainties in Measurements

This section addresses the general considerations for expressing uncertainties in measurements based on the standardised guide DS/ISO/IEC GUIDE 98-3 [41].

It is important to recognise that a measurement result represents an approximation or estimate of the true value of the measurand. Thus, the result is only considered complete when including a statement of the associated uncertainty. Moreover, measurements are also subject to imperfections leading to errors in the measurement result. These errors can be categorised into two components: random and systematic.

Random errors occur from the influence of unpredictable or stochastic temporal and spatial variations. The effect of random errors can typically be reduced by increasing the number of observations, as their expected value tends to zero. However, both random and systematic errors cannot be entirely eliminated. Nevertheless, a correction can be applied to reduce the systematic effect, assuming the expected value of the error is zero after the correction.

In practice, there are various sources of uncertainties, including the following stated in [41]:

- Incomplete definition of the measurand
- Imperfect realisation of the definition of the measurand
- Non-representative sampling - the sample measured may not represent the defined measurand
- Inadequate knowledge of the effects of environmental conditions on the measurement or imperfect measurement of environmental conditions
- Personal bias in reading analogue instruments
- Finite instrument resolution or discrimination threshold
- Inexact values of measurement standards and reference materials
- Inexact values of constants and other parameters obtained from external sources and used in the data-reduction algorithm
- Approximations and assumptions incorporated in the measurement method and procedure
- Variations in repeated observations of the measurand under apparently identical conditions

Given that the evaluation of uncertainties relies on potentially incomplete mathematical models, it is essential to conduct repeated measurements where all relevant quantities are varied as extensively as practically possible.

The evaluation of uncertainty is classified into Type A and Type B. Type A uncertainty is determined through statistical estimation using the variance of repeated observations. On the other hand, Type B uncertainty is based on available knowledge, which will not be discussed in detail here. In Type A evaluation of the standard uncertainty, the arithmetic mean ($\bar{q}$), also known as the average, is often considered the best estimate of the expected value (μ_q) of a randomly varying quantity (q). This estimation is based on n independent observations:

$$\bar{q} = \frac{1}{n}\sum_{k=1}^{n} q_k \tag{A.1}$$

The random variations of the individual observations (q_k) can be described by the variance (σ^2) of the probability distribution of q. This can be estimated by $s^2(q_k)$ which is the experimental variance:

$$s^2(q_k) = \frac{1}{n-1}\sum_{j=1}^{n} (q_j - \bar{q})^2 \tag{A.2}$$

This is alongside $s(q_k)$, its positive square root, termed the experimental standard deviation. It characterises the dispersion of observed values about their mean. The variance of the mean, $\sigma^2(\bar{q}) = \sigma^2/n$, is best estimated by:

$$s^2(\bar{q}) = \frac{s^2(q_k)}{n} \tag{A.3}$$

Quantifying how well $\bar{q}$ estimates the expectation (μ_q), this experimental variance of the mean and $s(\bar{q})$, the experimental standard deviation of the mean, may be used as a measure of the uncertainty.

The degrees of freedom, defined as "the number of terms in a sum minus the number of constraints on the terms of the sum", are $v = n-1$ in the case of the Type A standard uncertainty based on $s(\bar{q})$.

In some cases, it may be preferred to report the measure of uncertainty with a certain level of confidence. By applying a coverage factor, the so-called expanded uncertainty may be expected to encompass a large fraction of the distribution of values. The specific value of the coverage factor (k_p), producing a level of confidence (p), can be specifically calculated. However, a common value used is $k = 2$ giving a level of confidence of 95.45 %.

Furthermore, a better approximation can be achieved by using the t-distribution, utilising the degrees of freedom to correct for the small number of repeated observations. As an example, a measurement with ten repeated observations results in nine degrees of freedom and consequently a coverage factor of $k = 2.32$ for a level of confidence of 95.45 %.

A.2 Evaluation of Reference Hydrophones

The purpose of these measurements is to test the selected reference setup used for both calibration and field measurements. The following tests are completed:

- Calibrator Level: Measure the microphone output in the calibrator with the standard and the three-dimensional (3D)-printed coupler to determine the output levels.
- Hydrophone Sensitivities: Measure the hydrophone output voltage with the 3D-printed coupler to obtain the hydrophone sensitivities.
- Noise Floor: Measure the noise floor based on inherent noise to determine the limitations of the setup.
- Coupler Comparison: Measure the second 3D-printed coupler for validation by comparison with the first and determine the deviation.

A.2.1 Setup

The reference setup for calibration is shown in Fig. A.2.1 and for field measurements in Fig. A.2.2, followed by a list of equipment in Tab. A.2.1. These setups are almost identical, however, the calibration setup uses a measurement microphone as a reference and the field setup uses both hydrophones. The recorder is replaced with a measuring device for testing.

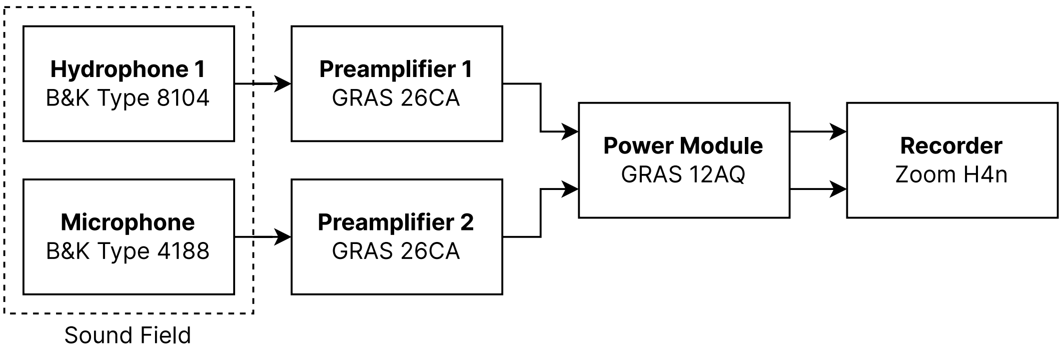

Figure A.2.1: Reference setup for calibration by comparison.

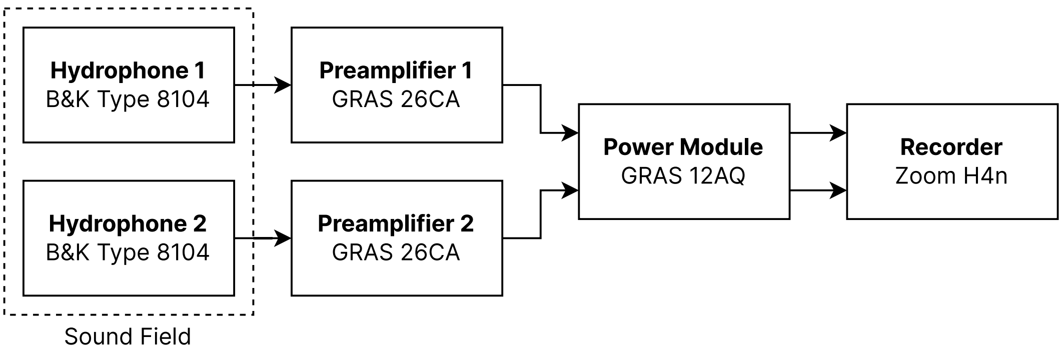

Figure A.2.2: Reference setup for field measurements.

Brand	Model	Description	AAU/Serial No.
GRAS	12AQ	Power module	126362/426811
GRAS	26CA	Preamplifier 1	108210/277020
GRAS	26CA	Preamplifier 2	108210/277294
B&K	Type 8104	Hydrophone 1	7841/1028242
B&K	Type 8104	Hydrophone 2	7842/1028243
B&K	Type 4188	Microphone	-/2250459
B&K	Type 4220	Pistonphone	08597-01/1404379
B&K	Type 2636	Measuring amplifier	08022/-
Fluke	289	Multimeter	64686/96350752
B&K	JJ 2617	Dummy microphone	-/-
-	-	3D-printed coupler 1	-/-
-	-	3D-printed coupler 2	-/-

Table A.2.1: List of equipment.

The first pictures in Fig. A.2.3 show the custom 3D-printed couplers used for calibration with the pistonphone as shown in Fig. A.2.4. The measurement equipment is shown in Fig. A.2.5 followed by the setup in Fig. A.2.6.

(a) Couplers seen from top

(b) Couplers seen from side

Figure A.2.3: 3D-printed coupler 1 (left) and 2 (right).

(a) Coupler 1 with microphone

(b) Coupler 2 without microphone

Figure A.2.4: 3D-printed couplers mounted in pistonphone.

(a) Multimeter **(b)** Measuring amplifier

Figure A.2.5: Voltage measurement equipment.

(a) Microphone in default coupler **(b)** Dummy microphone

Figure A.2.6: Microphone measurement setups.

A.2.2 Method/Procedure

All measurements are conducted in a quiet audiometry room (B4-103) in the laboratory. Hydrophones are fitted in the couplers and sealed with mounting putty when needed.

Output voltages are measured with the multimeter and measuring amplifier, the latter is solely used for obtaining the low-voltage noise floors. Microphone voltages are measured with the preamplifier and power module, while hydrophone voltages are measured at the end of the integral cable.

The inherent noise of the system is measured with a 50 pF dummy microphone attached to the preamplifier and power module, however, similar results were obtained with the hydrophone.

A.2.3 Results

Measurements are shown with expanded uncertainty (refer to Appx. A.1) from ten repeated measurements with a coverage factor of 2.32 based on a *t*-distribution with nine degrees of freedom defining an interval estimated to have a level of confidence of 95.45 %.

Calculations are done using the typical values and all values are root mean square (RMS) unless specified otherwise.

Calibrator Level

Specifications:

- Calibrator level: 124 dB re 20 μPa (± 0.15 dB) [physical chart]
- Preamplifier gain: −0.3 dB (typical) with 20 pF 1/2" dummy microphone [42]
- Power module gain: 0 dB (± 0.1 dB) from 20 Hz to 20 kHz [43]

Measurements:

- Microphone output (standard coupler): 978.40 mV (± 1.86 mV)
- Microphone output (3D-printed coupler 1): 866.06 mV (± 4.55 mV)

Calculations:

- Calibrator level (3D-printed coupler 1): 122.94 dB re 20 μPa (based on −1.06 dB average deviation from standard coupler)

Hydrophone Sensitivities

Specifications:

- Hydrophone sensitivity: −205 dB re 1 V/μPa (± 3 dB) with a frequency response from 0.1 Hz to 10 kHz with ± 1.5 dB re 250 Hz [22]

Measurements:

- Hydrophone 1 output (3D-printed coupler 1): 1.44 mV (± 0.02 mV)
- Hydrophone 2 output (3D-printed coupler 1): 1.50 mV (± 0.01 mV)

Calculations:

- Hydrophone 1 sensitivity: −205.78 dB re 1 V/μPa
- Hydrophone 2 sensitivity: −205.44 dB re 1 V/μPa

Noise Floor

Specifications:

- Preamplifier noise: ≤ 6 μV (typically 3.5 μV) linear from 20 Hz to 20 kHz
- Power module noise: < 2 μV (< 10 μV "when dominated by output noise") linear from 20 Hz to 20 kHz

Measurements:

- Power module outputs
  - 0 dB gain: 38 μV
  - 10 dB gain: 40 μV
  - 20 dB gain: 285 μV
  - 30 dB gain: 800 μV

Coupler Comparison

Measurements:

- Hydrophone 1 output (3D-printed coupler 2): 1.56 mV (± 0.03 mV)

Calculations:

- Calibrator level (3D-printed coupler 2): 123.61 dB re 20 µPa (based on 0.67 dB average deviation from 3D-printed coupler 1)

A.2.4 Notes

Low Frequency Limitations

A piezoelectric hydrophone requires a preamplifier with a high input impedance since it, together with the capacitance of the transducer, controls the electrical low-frequency limitations.

A simplified equivalent circuit with the hydrophone output voltage (V), free capacitance (C_f), and cable capacitance (C_C) is shown in Fig. A.2.7. Alongside this is a reduced circuit with the open circuit output voltage ($V_t = V_C$), total capacitance ($C_t = C_f + C_C$), as well as the preamplifier input impedance (R_i) [21].

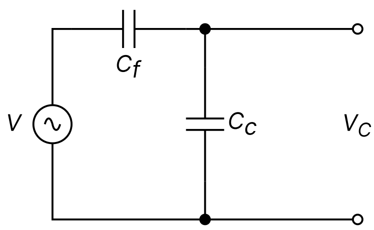

(a) With cable capacitance

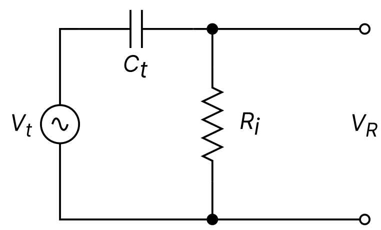

(b) With preamplifier input resistance

Figure A.2.7: Hydrophone equivalent diagrams.

The lower limiting cut-off frequency can be calculated using

$$f_C = \frac{1}{2\pi R_i C_t} \tag{A.4}$$

With the following values: C_t = 7800 pF and R_i = 10 GΩ, given in the datasheets, this results in f_C = 0.002 Hz. Any additional capacitance from cables would lower this even further. In conclusion, this will not limit the performance of the reference setup.

A.3 Evaluation of Custom Hydrophones

The purpose of these measurements is to measure the performance of the custom hydrophones and compare them with the reference hydrophones.

A.3.1 Setup

The test setup for calibrated measurements is shown in Fig. A.3.1 followed by a list of equipment in Tab. A.3.1.

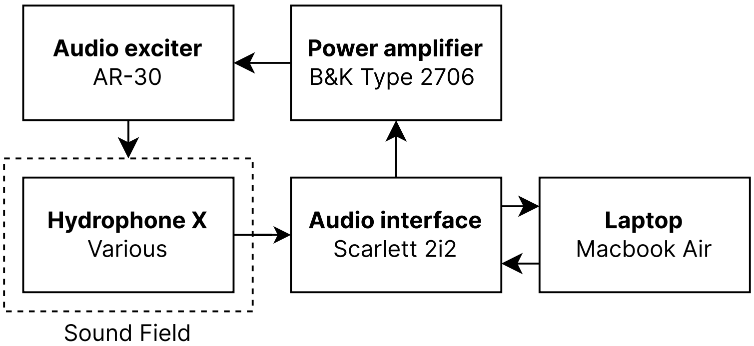

Figure A.3.1: Test setup for calibrated measurements.

Brand	Model	Description	AAU/Serial No.
Apple	Macbook Air	Laptop	-/C02GHVURQ6L4
Focusrite	Scarlett 2i2	Audio interface	-/Y8EF52B1370ADB
B&K	Type 2706	Power amplifier	64654/462201
Monacor	AR-30	Audio exciter	-/-
B&K	Type 8104	Hydrophone 1	7841/1028242
B&K	Type 8104	Hydrophone 2	7842/1028243
-	Piezoceremic	Hydrophone 3	-/-
-	Electret	Hydrophone 4	-/-
B&K	Type 4220	Pistonphone	08597/1404379
Fluke	37	Multimeter	08287/04325187
Fluke	289	Multimeter	64687/96350754
-	-	3D-printed coupler 2	-/-

Table A.3.1: List of equipment.

Calibration

The reference hydrophone is calibrated using the pistonphone and 3D-printed coupler as shown in Fig. A.3.2.

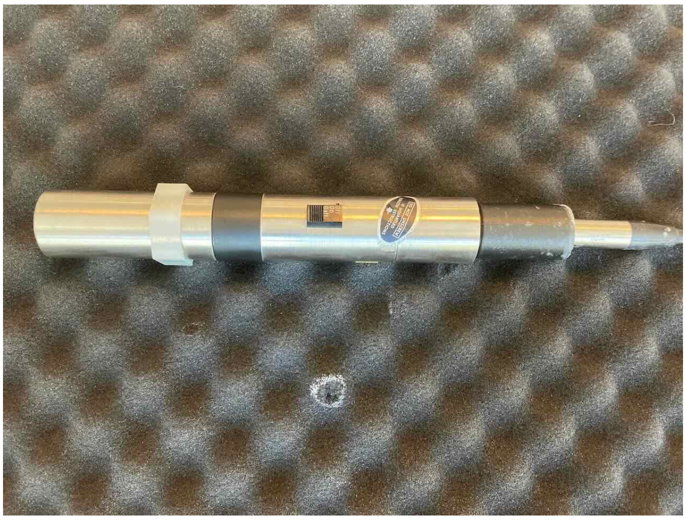

Figure A.3.2: Laboratory calibration setup in the waiting room (B4-101).

Measurements

Measurements are made in a 90 L mortar bucket with the largest dimensions of 80 cm × 50 cm × 31.5 cm, filled with 60 L of tap water. The reference hydrophone setup is shown in Fig. A.3.3 followed by the custom hydrophones in Fig. A.3.4.

A ground connection was added to reduce power frequency noise when measuring with the reference hydrophones and a weight was used to submerge the custom hydrophones, both of which are depicted in Fig. A.3.5.

An audio exciter is attached to the end of the bucket as seen in Fig. A.3.6 and utilised as the sound source for the measurements. This is done due to insufficient low-frequency sound generation when using the reference hydrophone as a projector (see Fig. A.3.7).

(a) Top-view **(b)** Close-up

Figure A.3.3: Reference hydrophone placed in the corner of the mortar bucket.

(a) Piezo **(b)** Electret

Figure A.3.4: Custom hydrophones placed in the corner of the mortar bucket.

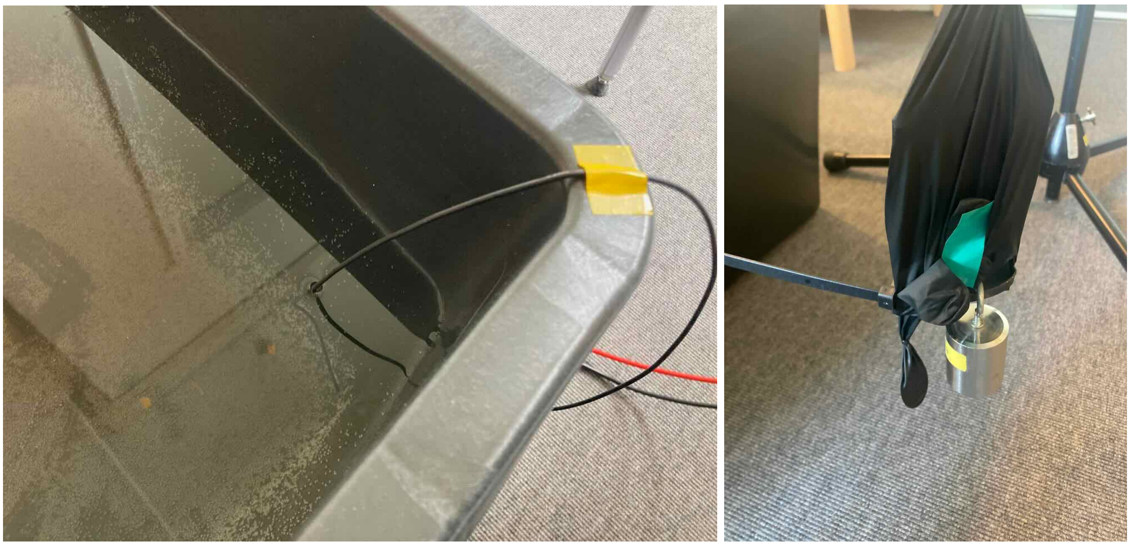

(a) Ground wire **(b)** Added weight

Figure A.3.5: Hydrophone ground connection wire and additional weight for custom hydrophones.

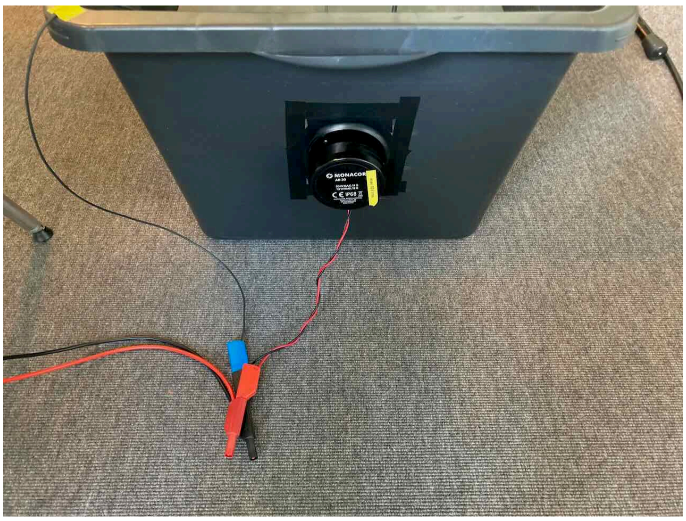

Figure A.3.6: Audio exciter mounted on the end of the mortar bucket.

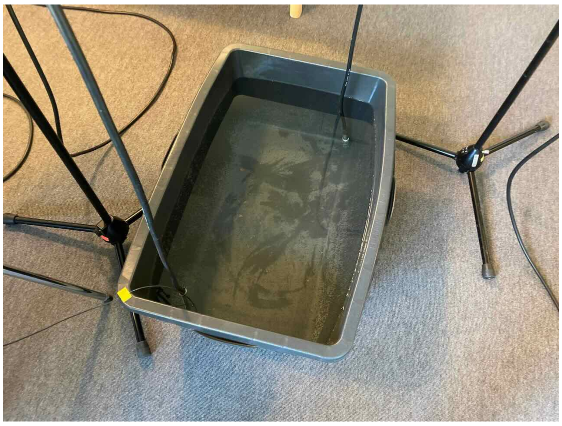

(a) Top-view (both)

(b) Close-up (projector)

Figure A.3.7: Reference hydrophones used as both projector and receiver.

A.3.2 Method/Procedure

All measurements are made using the acoustic measurement software REW 5.20.13 [44]. The reference hydrophones use the instrument input of the audio interface, while the custom hydrophones go through the internal microphone preamplifier.

Noise measurements are made with the RTA tool using the following settings:

- Mode: Spectrum
- FFT Length: 64k
- Averages: 32
- Window: Hann
- Overlap: 87.5 %

Frequency response measurements are made using the following settings:

- Type: SPL
- Start Freq: 1 Hz
- End Freq: 22 kHz
- Level: −12 dBFS (equal to 2.79 Vrms at 250 Hz)
- Method: Sweep
- Length: 128k
- Repetitions: 8
- Duration: 21.8 s (total)
- Sample rate: 48 kHz

The following procedure is used for the calibration of the measurement system with hydrophone 1:

1. Hydrophone 1 is inserted into the 3D-printed coupler and mounted on the pistonphone calibrator (output is 124 dB re 20 µPa at 250 Hz).
2. Input gain is adjusted on the audio interface with adequate headroom (min. −19 dBFS to ensure no clipping at 140 dB re 20 µPa).
3. Hydrophone 1 is placed in the lower corner of the mortar bucket (opposite side to the audio exciter) with 2 cm distance to all boundaries.

4. Pressure field of 112 dB re 20 μPa is generated underwater at 250 Hz with the audio exciter.
5. Output voltage is measured across the audio exciter (2.79 Vrms equal to −12 dBFS).

The following procedure is used for the measurements and repeated for all four hydrophones.:

1. Hydrophone is placed in the lower corner of the mortar bucket (opposite side to the audio exciter) with 2 cm distance to all boundaries.
2. Pressure field of 112 dB re 20 μPa is generated underwater at 250 Hz with the audio exciter.
3. Input gain is adjusted on the audio interface with adequate headroom (min. −19 dBFS to ensure no clipping at 140 dB re 20 μPa).
4. Noise floor with the hydrophone is measured.
5. Frequency response of the hydrophone is measured.
6. The hydrophone is removed, re-positioned and its frequency response is measured again.
7. Item 6 is repeated for at total of three measurements.

A.3.3 Results

Sound pressure level (SPL), displayed on the y-axis of the plots, are decibels relative to 20 μPa. All hydrophone sound pressure levels are pressure field calibrated underwater to 112 dB SPL at 250 Hz.

Initial measurements are made using the reference hydrophone 2 as a projector, however, this was insufficient at low frequencies so an audio exciter was used instead. A comparison of the two measurement methods is shown in Fig. A.3.8 and A.3.9.

Figure A.3.10 and A.3.11 show the noise floor measurements. The repeated frequency response measurements of the reference hydrophone 2, piezoelectric hydrophone and electret hydrophone are shown in Fig. A.3.12, A.3.13 and A.3.14, all compared to the first measurement of hydrophone 1. A comparison of all frequency responses is shown in Fig. A.3.15 and A.3.16.

Due to the SPL calibration happening on a slope between a peak and dip, the frequency responses are somewhat misaligned. Figure A.3.17 shows the aligned frequency responses based on an average over two octaves, centred at 250 Hz. The relative difference of the three hydrophones from hydrophone 1 is shown in Fig. A.3.18 and A.3.19, and again presented after alignment in Fig. A.3.20.

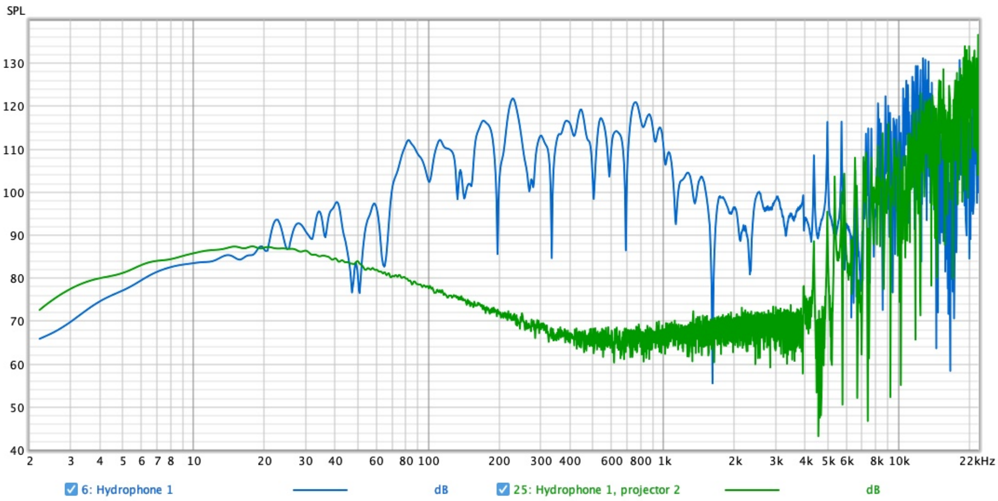

Figure A.3.8: Frequency responses of hydrophone 1 with the audio exciter and hydrophone 2 as the projector.

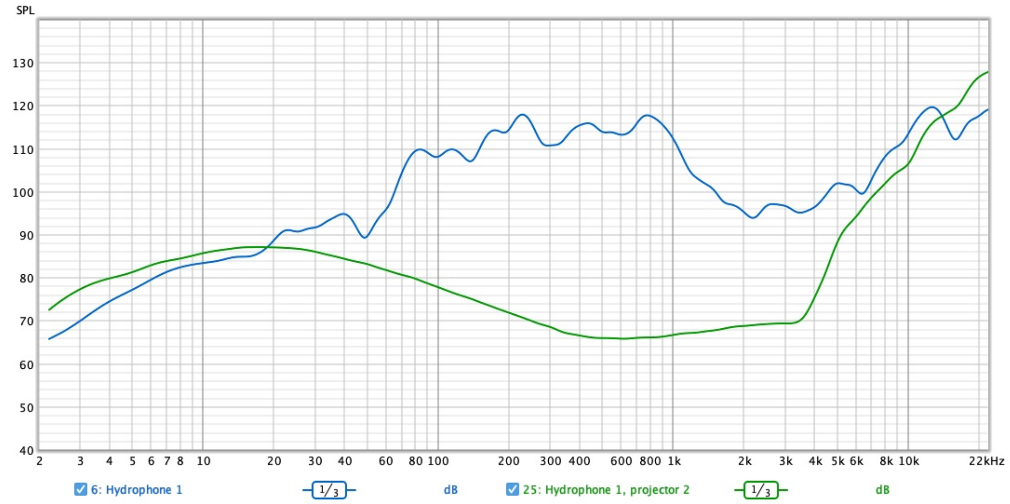

Figure A.3.9: Frequency responses of hydrophone 1 with the audio exciter and hydrophone 2 as the projector (1/3 octave smoothing).

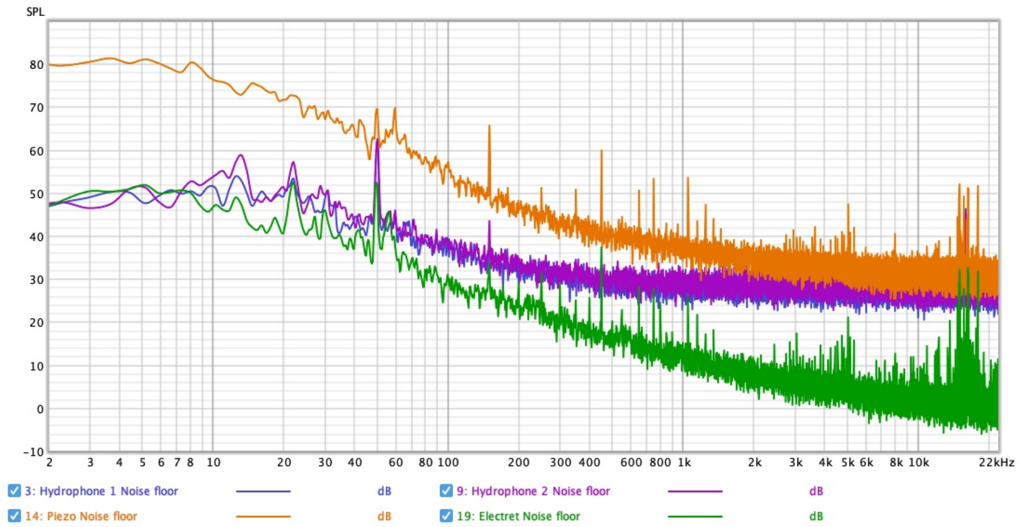

Figure A.3.10: Noise floor spectra measured with all hydrophones.

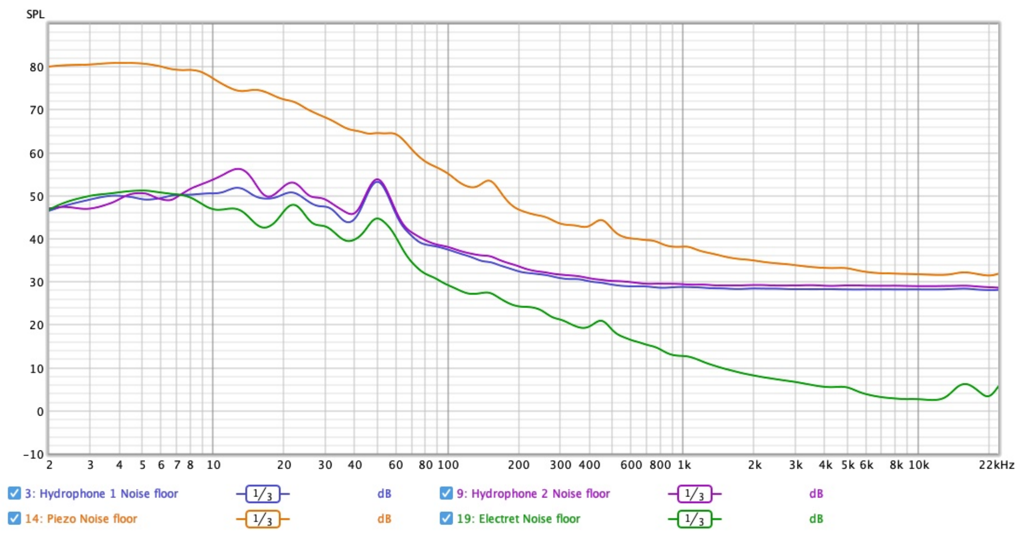

Figure A.3.11: Noise floor spectra measured with all hydrophones (1/3 octave smoothing).

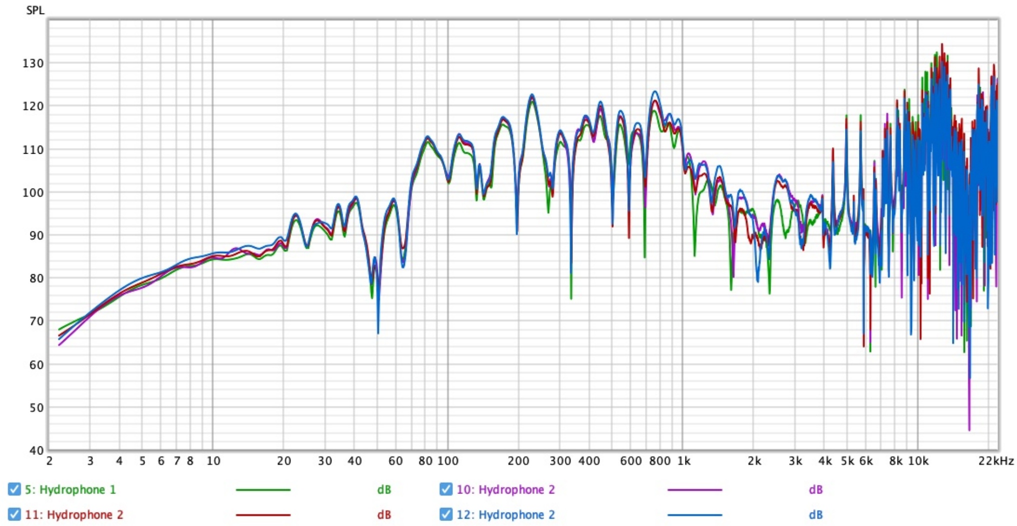

Figure A.3.12: Frequency responses of hydrophone 2.

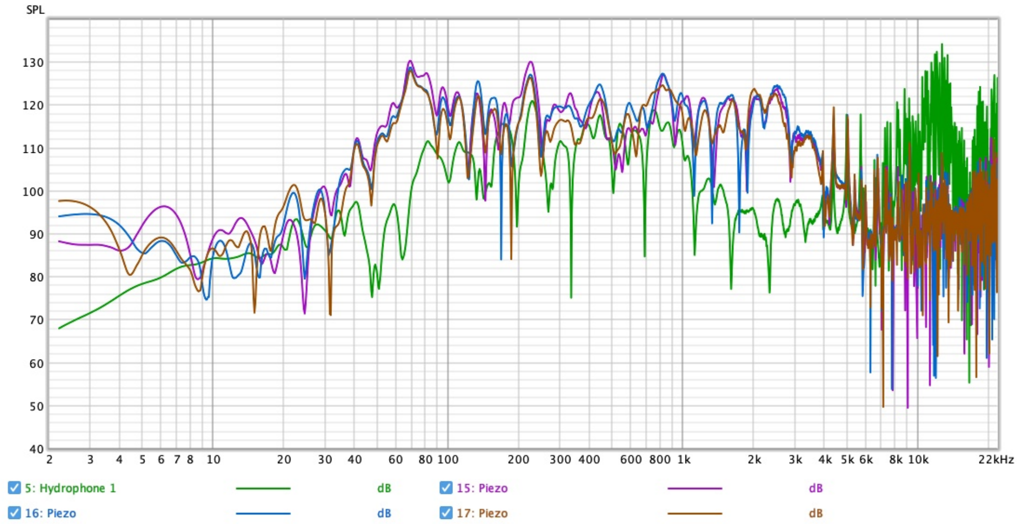

Figure A.3.13: Frequency response of custom piezoelectric hydrophone.

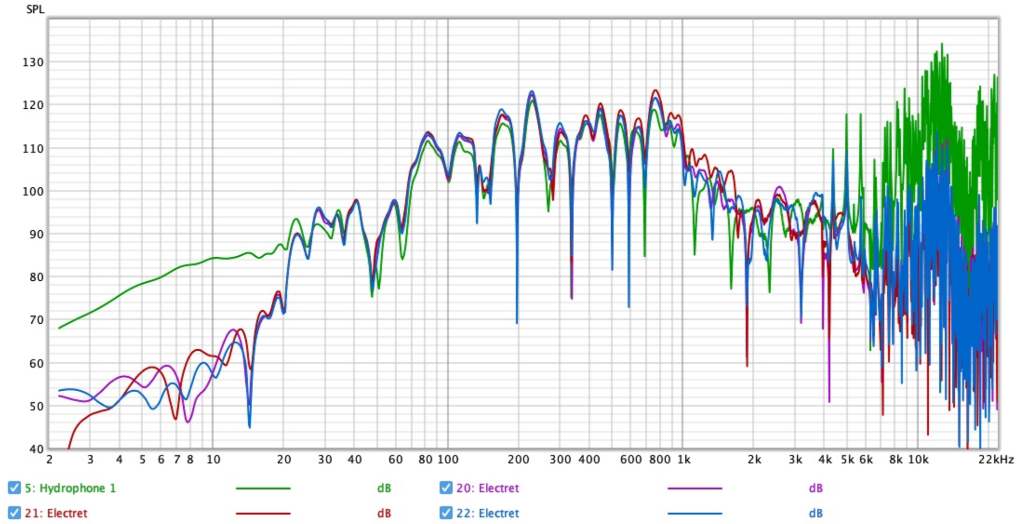

Figure A.3.14: Frequency response of custom electret hydrophone.

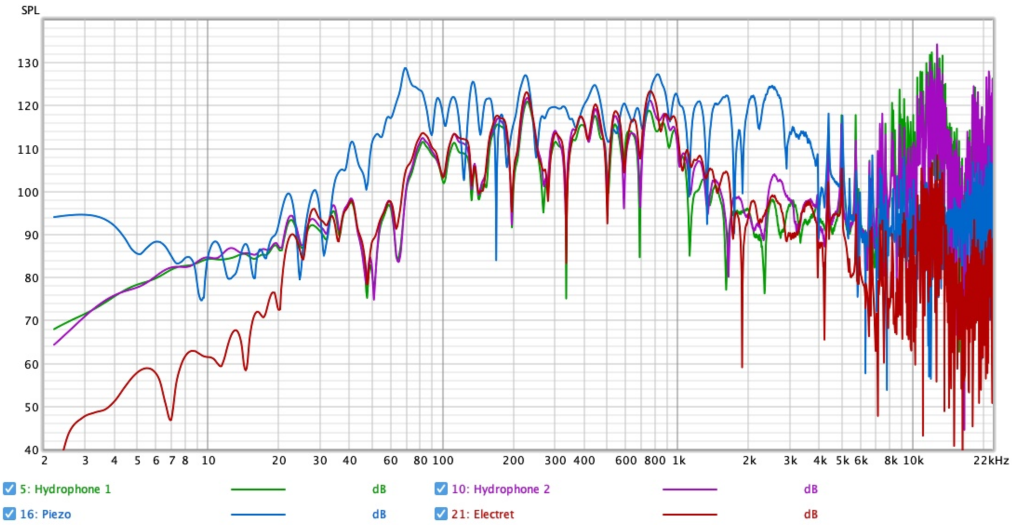

Figure A.3.15: Frequency response of all hydrophones.

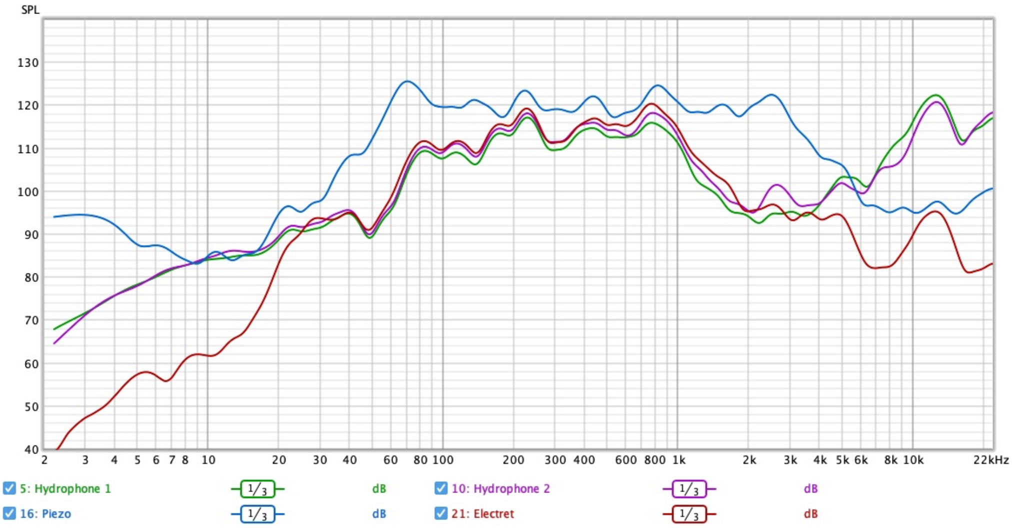

Figure A.3.16: Frequency response of all hydrophones (1/3 octave smoothing).

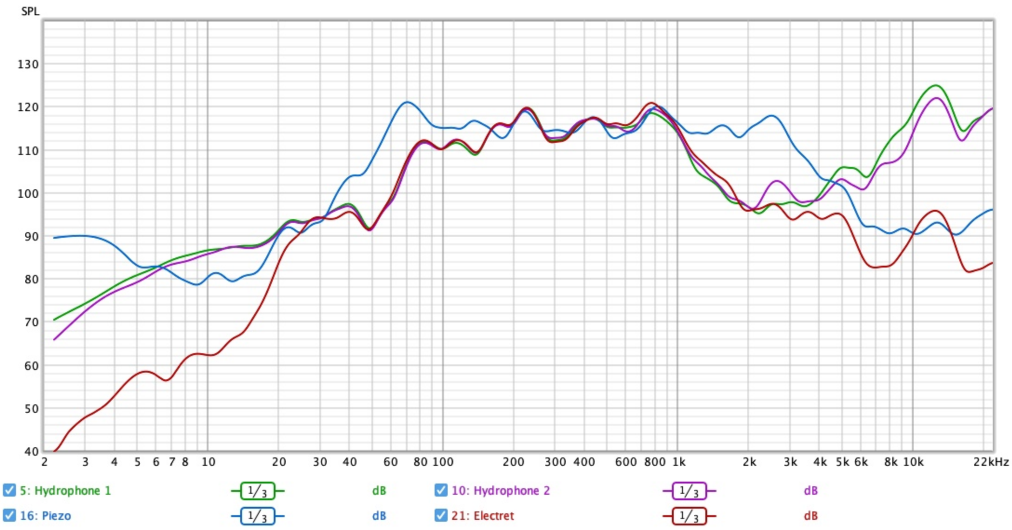

Figure A.3.17: Frequency response of all hydrophones (1/3 octave smoothing and aligned).

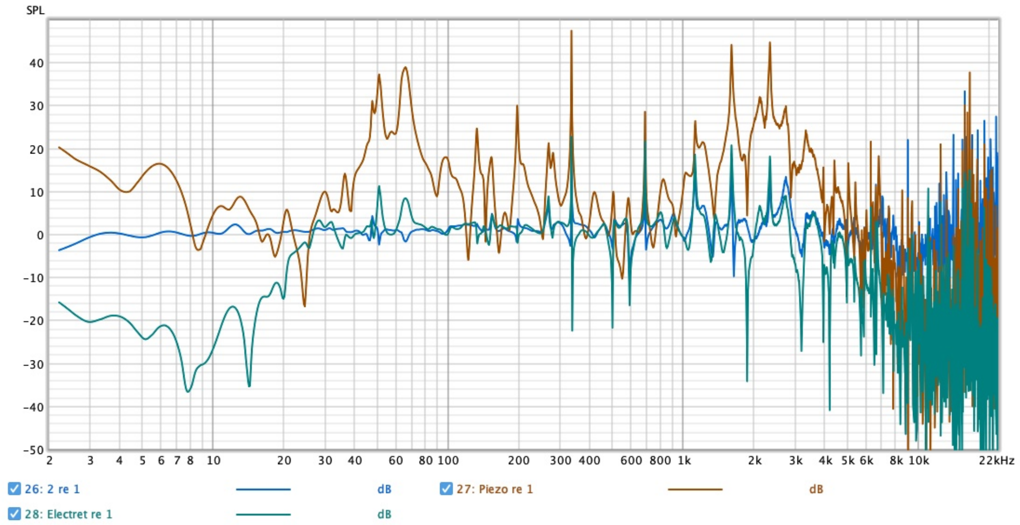

Figure A.3.18: Frequency response difference of all hydrophones.

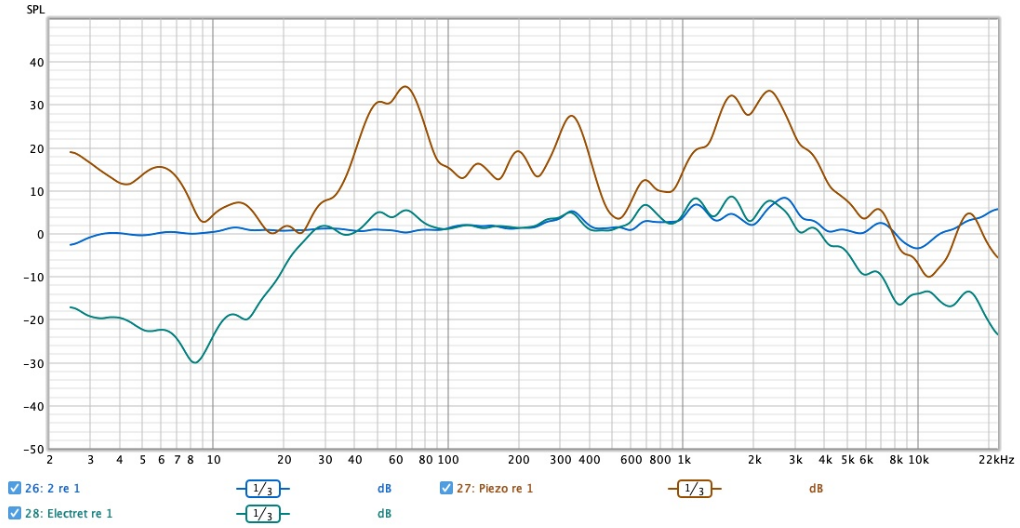

Figure A.3.19: Frequency response difference of all hydrophones (1/3 octave smoothing).

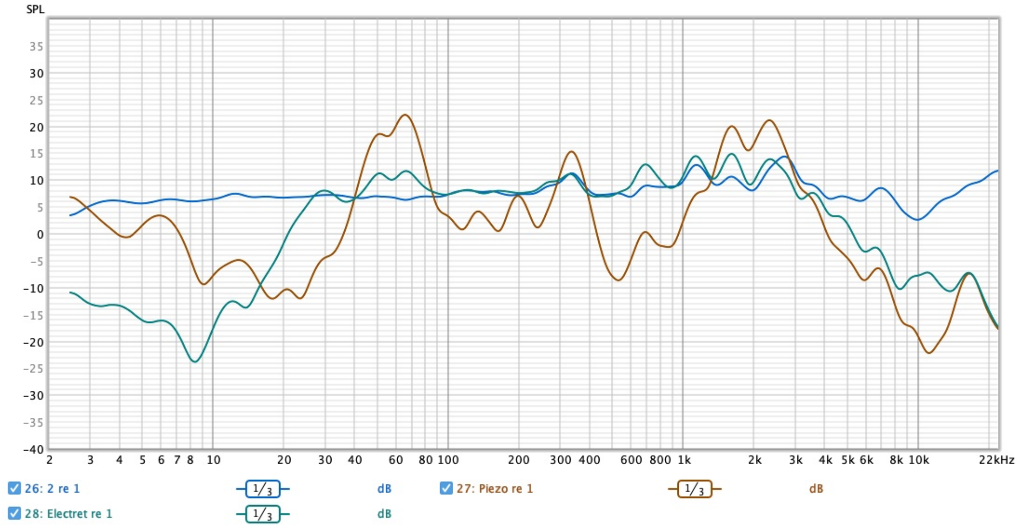

Figure A.3.20: Frequency response difference of all hydrophones (1/3 octave smoothing and aligned).

B Field Measurements

B.1 Reference Measurements in Aalborg Harbour

The purpose of these measurements is to collect field measurements of a person jumping into the water as well as the background noise in Aalborg Harbour.

These measurements are conducted in collaboration with a 2nd-semester group studying the Master's programme in Computer Engineering at Aalborg University.

B.1.1 Setup

The setup for the field measurements is shown in Fig. B.1.1 followed by a list of equipment in Tab. B.1.1.

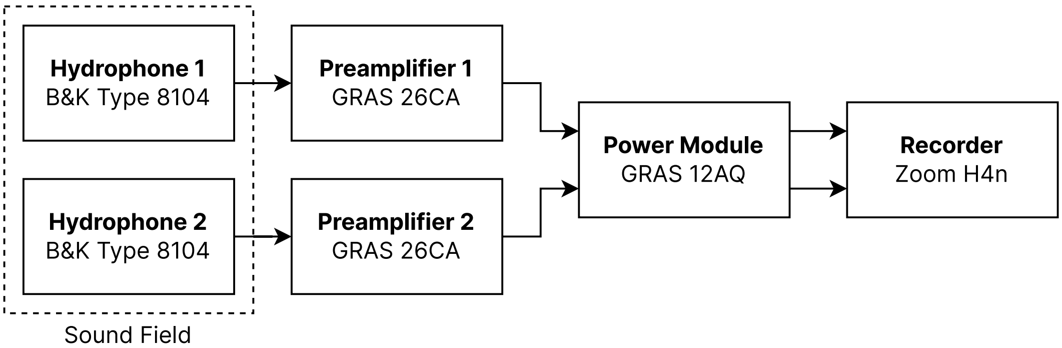

Figure B.1.1: Setup for field measurements.

Brand	Model	Description	AAU/Serial No.
Zoom	H4n	Recorder	86309/00354339
GRAS	12AQ	Power module	126362/426811
GRAS	26CA	Preamplifier 1	108210/277020
GRAS	26CA	Preamplifier 2	108210/277294
B&K	Type 8104	Hydrophone 1	7841/1028242
B&K	Type 8104	Hydrophone 2	7842/1028243
B&K	Type 4220	Pistonphone	08597/1404379
-	-	three-dimensional (3D)-printed coupler 2	-
MONACOR	SM-4	Sound level meter	02126-00/01019

Table B.1.1: List of equipment.

Calibration

Both hydrophones are calibrated in a quiet listening cabin measured at 45 to 55 dB(C) in the laboratory at Aalborg University. The setup is shown in Fig. B.1.2.

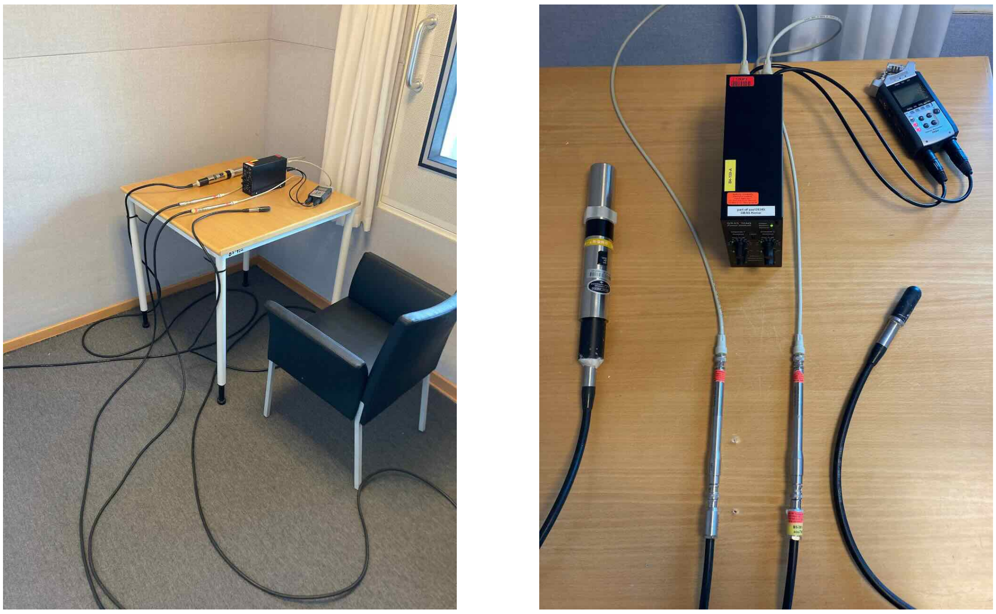

(a) Overview **(b)** Close-up

Figure B.1.2: Laboratory calibration setup in listening cabin B (B5-104).

Measurements

These field measurements are conducted in the eastern part of Aalborg in the vicinity of Østre Havn. A nautical map of the area is displayed in Fig. B.1.3. This is followed by a picture taken on-site (see Fig. B.1.4).

Hydrophone 1 is mounted on a rescue ladder 0.28 m from the wall and hydrophone 2 is freely hanging from the slightly overhanging edge of the harbour (see Fig. B.1.5). Both hydrophones are submerged approximately 1 m below the surface and there is 2.15 m from the surface to the edge of the harbour. The hydrophones are separated by 12.6 m with the remaining equipment (see Fig. B.1.6) placed in between (see Fig. B.1.7). The test subject has a weight of 63 kg, height of 1.78 m, and is dressed in a wetsuit (see Fig. B.1.8). Several jumps are made and an example with four frames from a video is displayed in Fig. B.1.9.

During the measurements, the highest 10 min average wind speed was 13 m/s [45] and the temperature of the water was 3.2 °C [11].

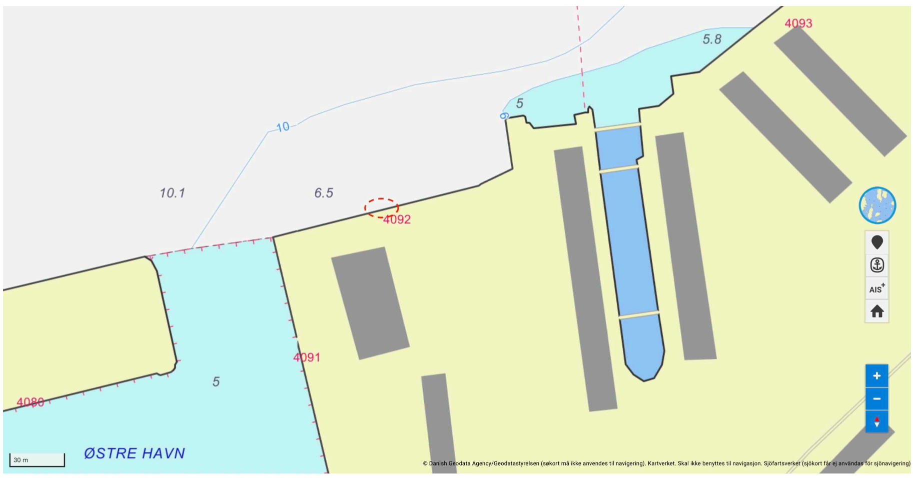

Figure B.1.3: Nautical map of the measurement location (highlighted with a red dashed ellipse).

Figure B.1.4: Location overview (taken inwards).

(a) Hydrophone 1 (rescue ladder)

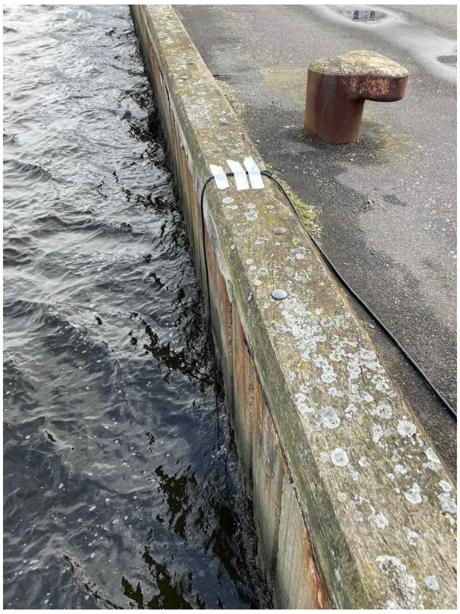

(b) Hydrophone 2 (freely hanging)

Figure B.1.5: Mounting of the hydrophones at the harbour.

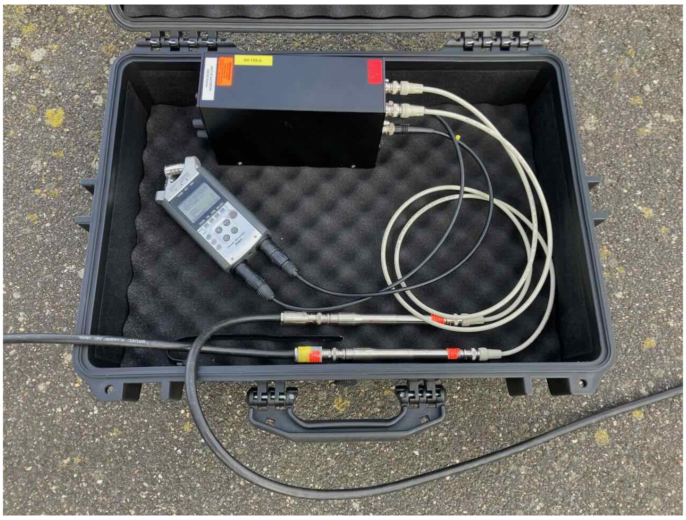

Figure B.1.6: Close-up of the case with measurement equipment.

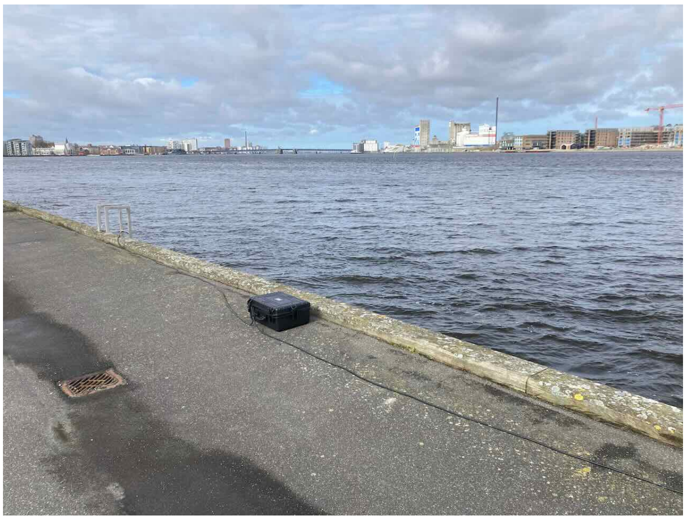

Figure B.1.7: Overview of the case with measurement equipment.

Figure B.1.8: Test subject before a jump.

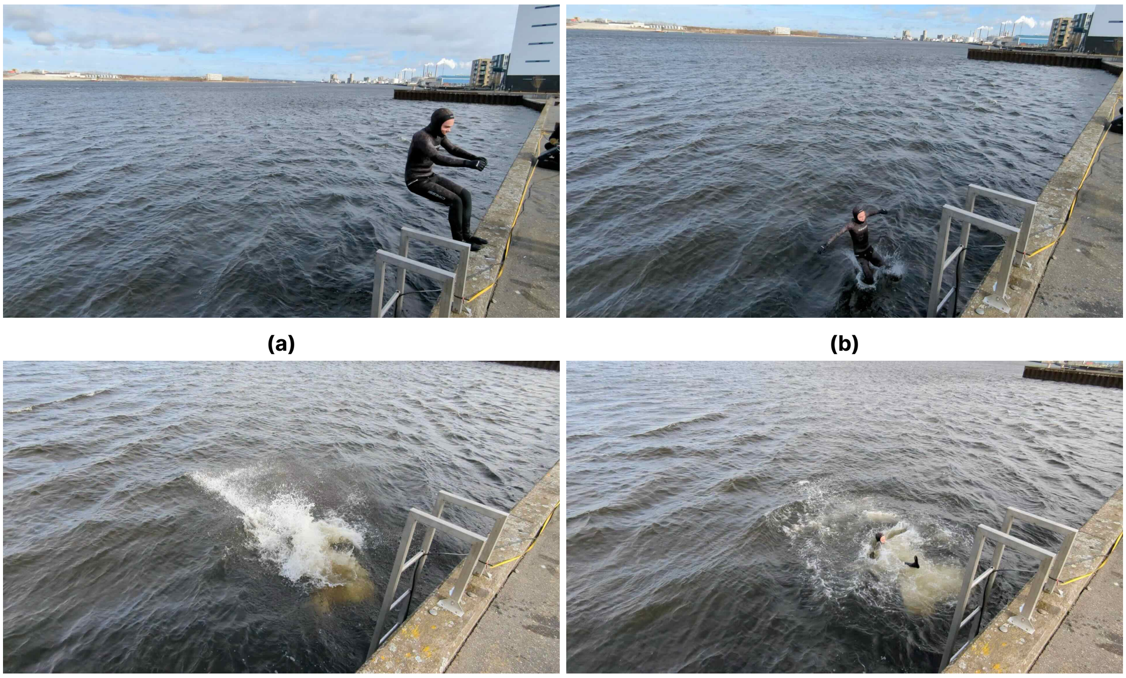

(a)

(b)

(c)

(d)

Figure B.1.9: Four frames from a video taken of one of the jumps.

B.1.2 Method/Procedure

All recordings are made in stereo at 48 kHz/16-bit with an input level of 30 and using two different gain settings on the power module: 0 dB (low) and 20 dB (high).

The following calibration procedure is performed for each hydrophone:

1. Hydrophone is inserted into the 3D-printed coupler and mounted on the pistonphone calibrator.
2. Output gain is adjusted on the power module.
3. Pistonphone calibrator is turned on.
4. Signal is recorded.

The following measurement procedure is performed:

1. Hydrophones are placed in the water.
2. Output gains are adjusted on the power module.
3. Signals are recorded.

A total of five jumps are made approximately 1 m out from the harbour at various distances to the hydrophones.

B.1.3 Results

All calculations and plots are made using Python 3.9.16 [46] and the following packages:

- NumPy 1.23.5 [47]
- Matplotlib 3.7.1 [48]
- SciPy 1.10.1 [49]
- librosa 0.10.0 [50]

Measurements are calibrated using a 10 s recording of the pistonphone calibration signal at each gain setting.

Recorded waveforms are shown with calibrated sound pressure.

Sound pressure levels are calculated using a fast time weighing of 125 ms which is implemented as an exponential moving average filter. The dashed line shows the average sound pressure level (SPL).

The spectrograms presented are made with a sample rate of 48 kHz and a 4096 point fast Fourier transform (FFT). This results in each frame having a duration of 85 ms and a frequency resolution of 11.7 Hz. Furthermore, a 50 % overlap is used and the spectrograms all have a 80 dB dynamic range.

The script and audio files for generating the visualisations can be found in 'Attachments/Field Measurements/Aalborg Harbour'. These selected clips from the recordings are presented in the figures below.

Low gain

Three jumps from 1 m, 2.5 m and 5 m are shown for both hydrophones in Fig. B.1.10, B.1.11 and B.1.12.

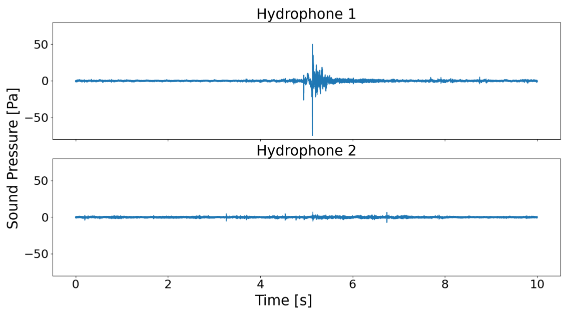

(a) Sound pressure

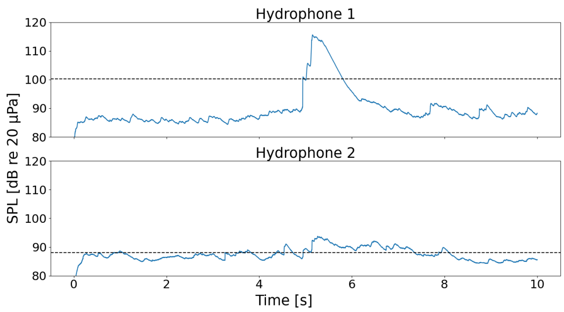

(b) SPL

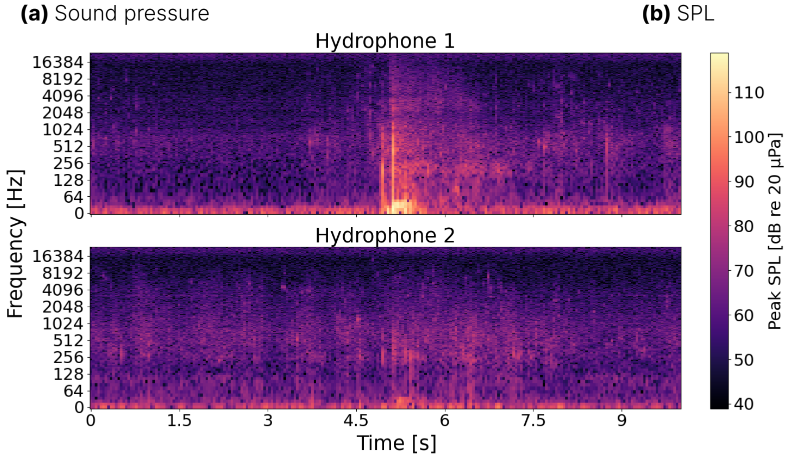

(c) Spectrogram

Figure B.1.10: Jump 1 m from hydrophone 1 and 11.6 m from hydrophone 2.

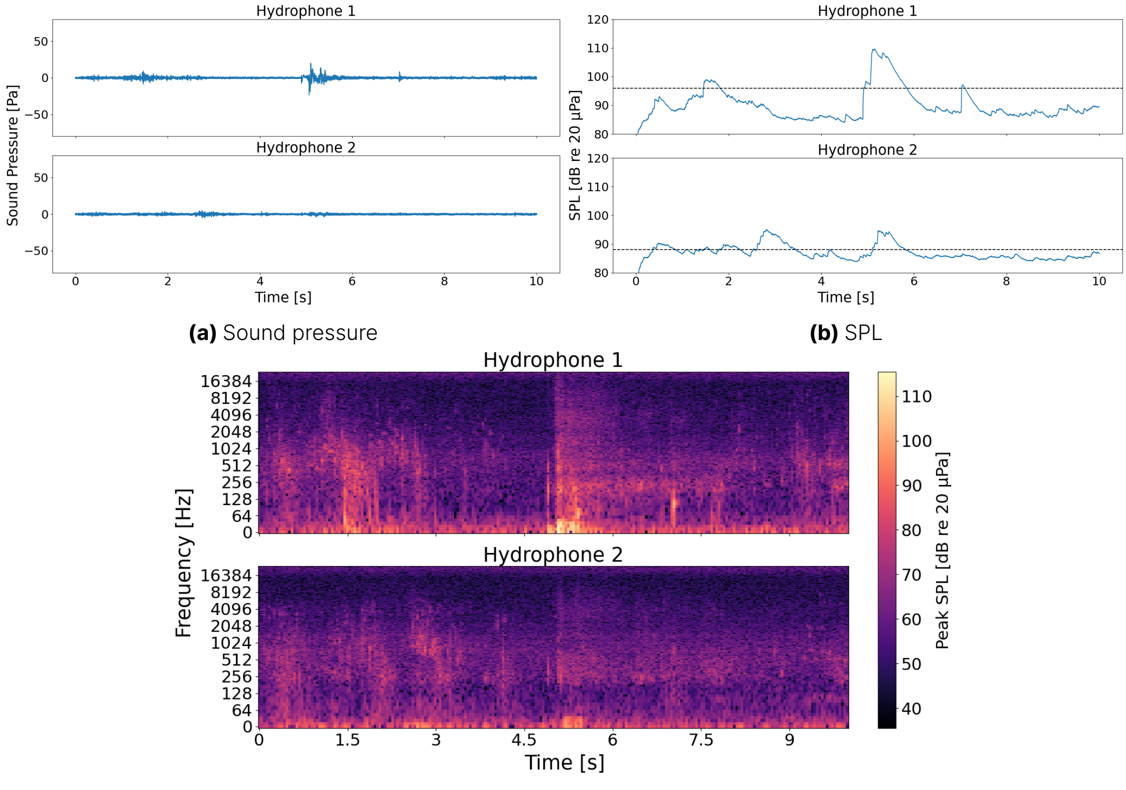

(a) Sound pressure **(b)** SPL

(c) Spectrogram

Figure B.1.11: Jump 2.5 m from hydrophone 1 and 10.1 m from hydrophone 2.

The two peaks just after 1.5 s and 7 s at hydrophone 1 in Fig. B.1.11 might be from the loose hydrophone hitting the harbour wall or accidental handling of the equipment.

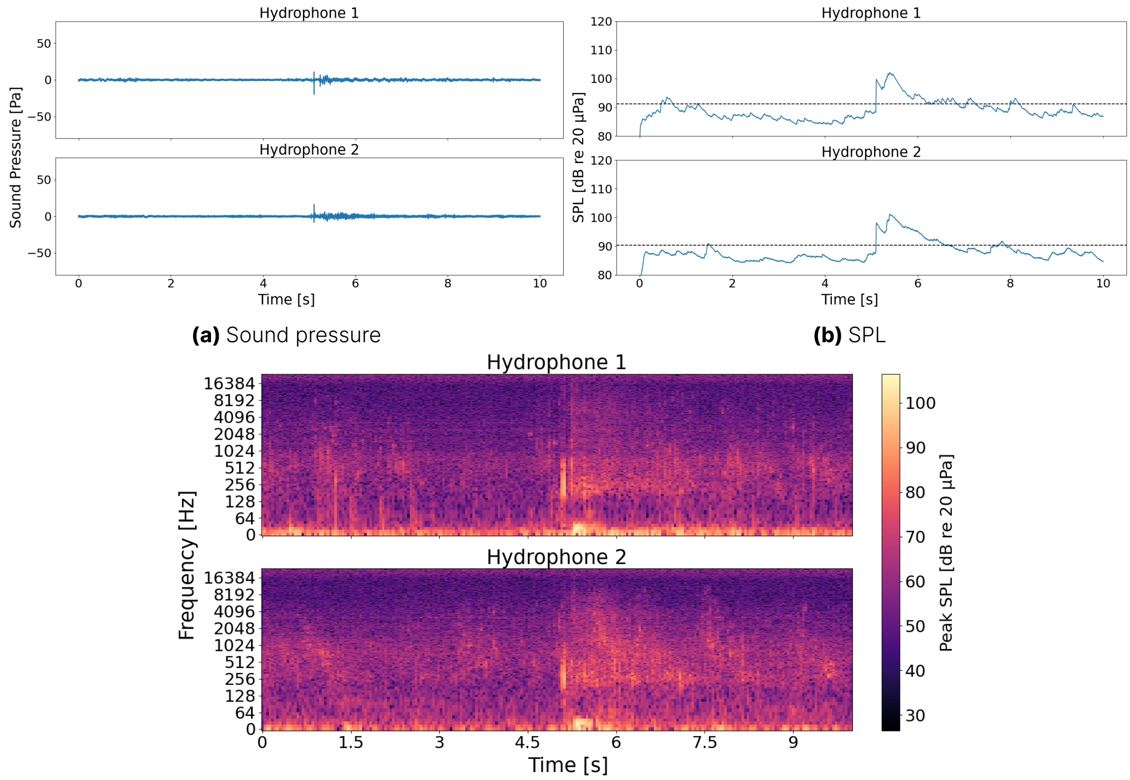

(a) Sound pressure **(b)** SPL

(c) Spectrogram

Figure B.1.12: Jump 5 m from hydrophone 1 and 7.6 m from hydrophone 2.

High gain

Two jumps from 1 m and 6 m and background noise is shown for both hydrophones in Fig. B.1.13, B.1.14 and B.1.15.

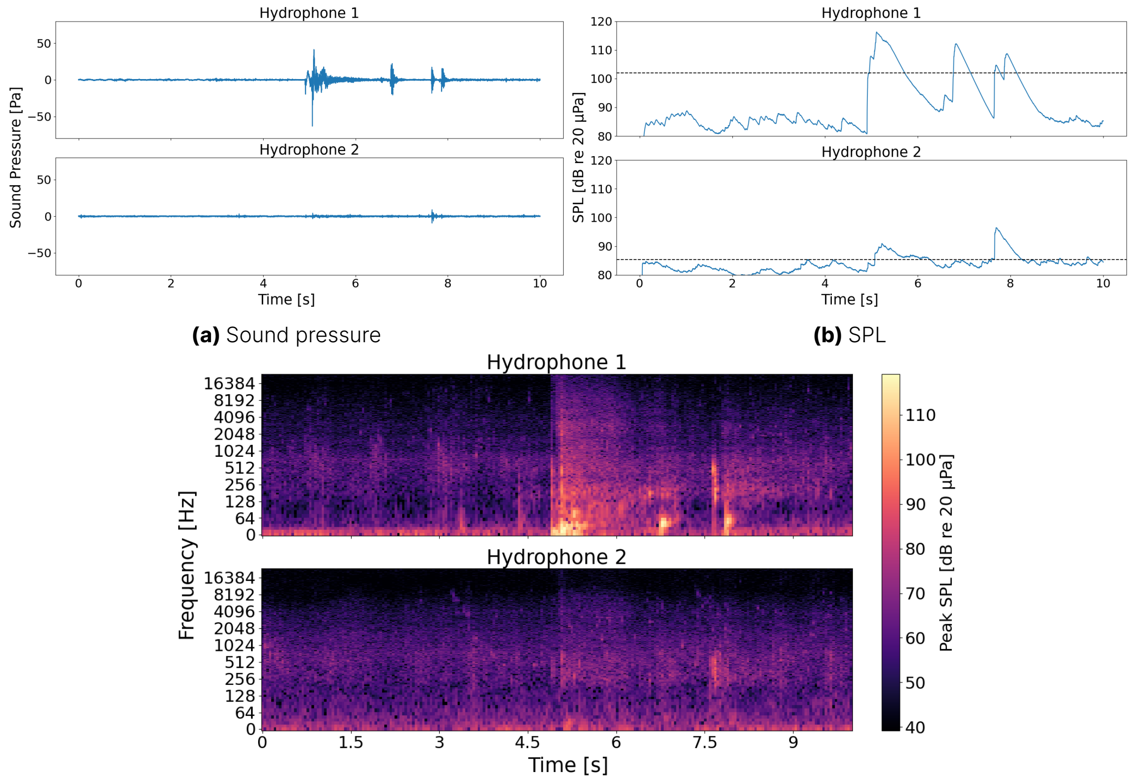

(a) Sound pressure

(b) SPL

(c) Spectrogram

Figure B.1.13: Jump 1 m from hydrophone 1 and 11.6 m from hydrophone 2.

The two peaks around 7 s and 8 s at the top plots in Fig. B.1.13 might be from the loose hydrophone hitting the harbour wall and the peak seen in both top and bottom just before 8 s is likely from accidental handling of the equipment.

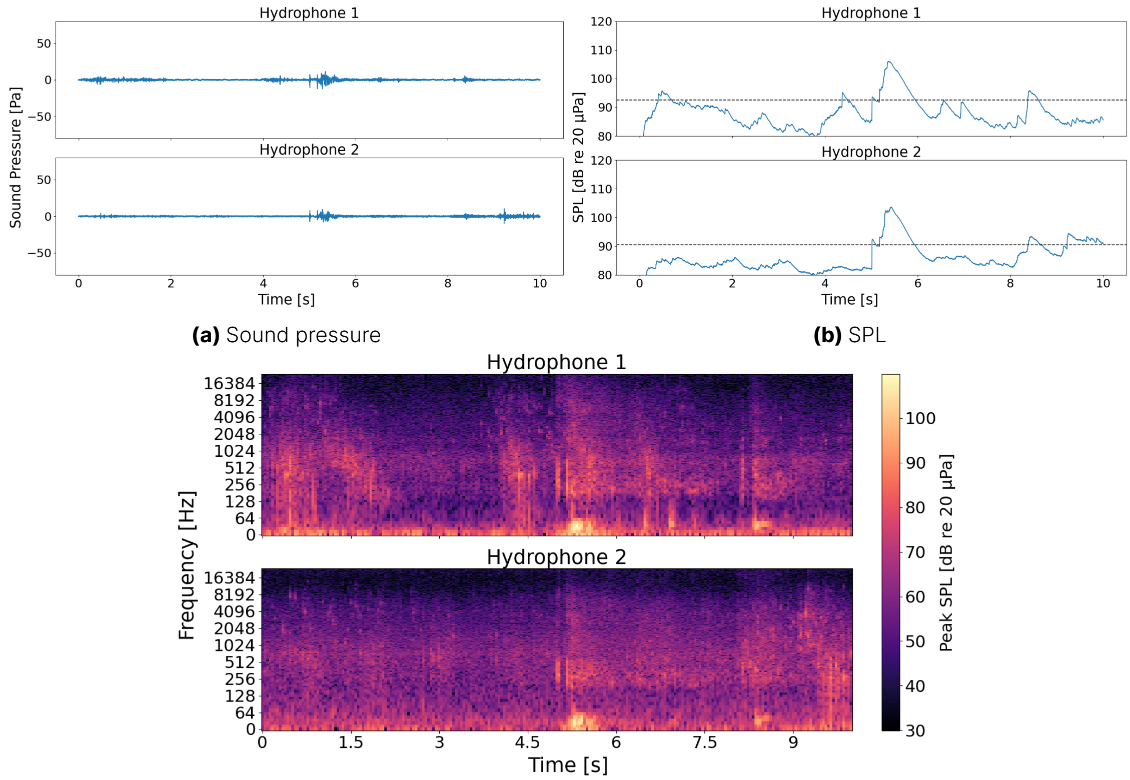

(a) Sound pressure

(b) SPL

(c) Spectrogram

Figure B.1.14: Jump 6 m from hydrophone 1 and 6.6 m from hydrophone 2.

The peaks that are seen after the jump from 6 s at the top plots in Fig. B.1.14 are from the test subject actively moving the arms around in the water. The peak seen after 8 s is likely due to accidental handling of the equipment.

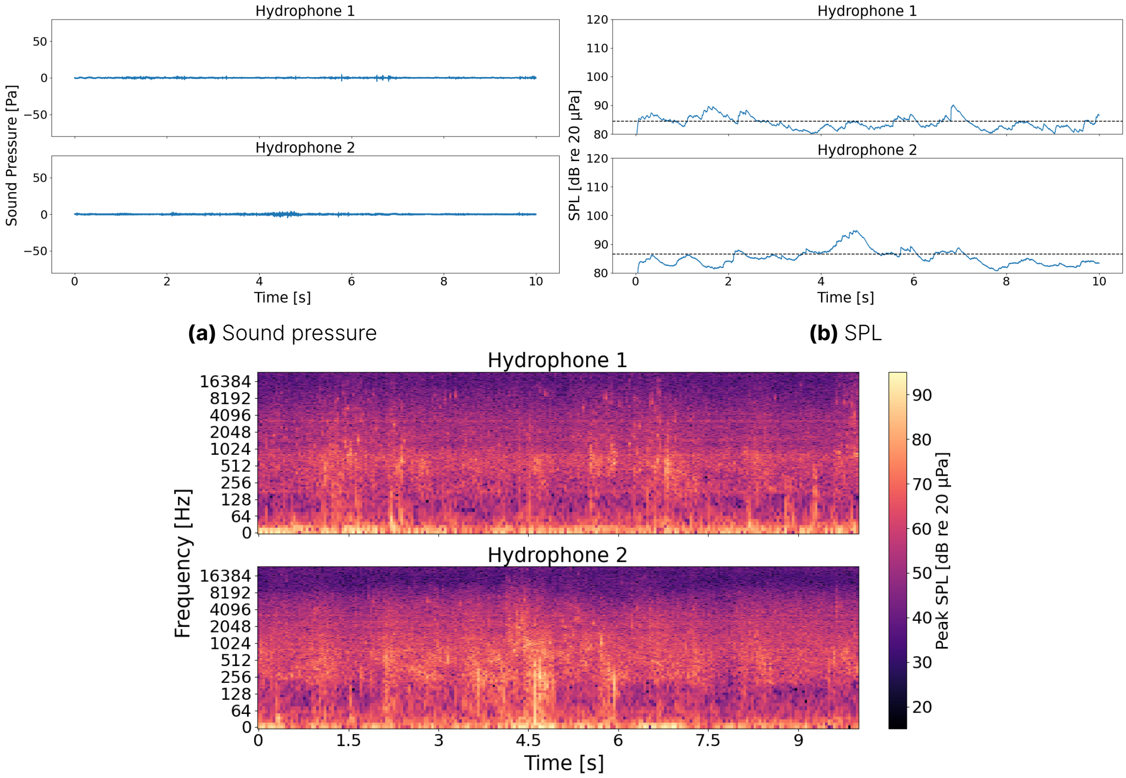

(a) Sound pressure **(b)** SPL

(c) Spectrogram

Figure B.1.15: Background noise with hydrophone 1 and with hydrophone 2.

B.2 Reference Measurements in Aarhus Harbour

The purpose of these measurements is to collect additional field measurements of the background noise and specific noise sources in Aarhus Harbour.

B.2.1 Setup

The setup for the field measurements is shown in Fig. B.2.1 followed by a list of equipment in Tab. B.2.1.

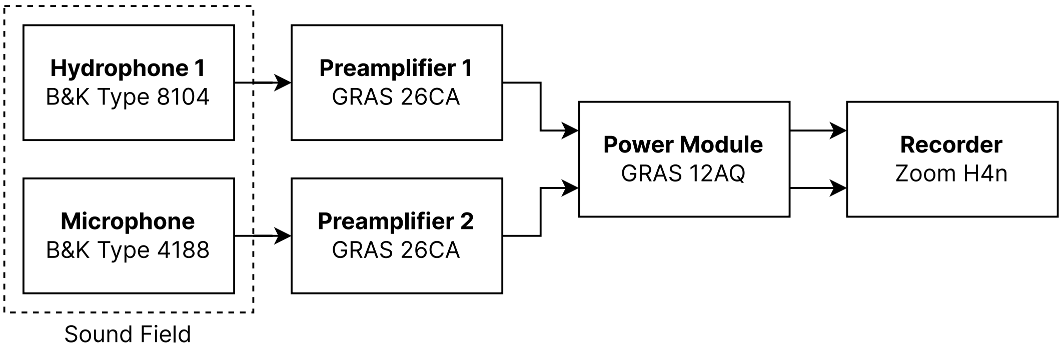

Figure B.2.1: Setup for field measurements.

Brand	Model	Description	AAU/Serial No.
Zoom	H4n	Recorder	86309/00354339
GRAS	12AQ	Power module	126362/426811
GRAS	26CA	Preamplifier 1	108210/277020
GRAS	26CA	Preamplifier 2	108210/277294
B&K	Type 8104	Hydrophone 1	7841/1028242
B&K	Type 4188	Microphone	-/2250459
B&K	Type 4220	Pistonphone	08597/1404379
-	-	3D-printed coupler 2	-

Table B.2.1: List of equipment.

Calibration

The hydrophone is calibrated in the laboratory at Aalborg University before and after the measurements. This setup is shown in Fig. B.2.2.

Figure B.2.2: Laboratory calibration setup in control room S (B4-113).

Measurements

The location used for the field measurements is Hunnørkajen which is connected to basins 1 and 2 in Aarhus Harbour. A nautical map of the area is displayed in Fig. B.2.3. This is followed by a picture taken on-site (see Fig. B.2.4).

The hydrophone is attached to a telescoping pole (see Fig. B.2.5) and mounted on a rescue ladder, flush with the wall due to its position in a 0.2 m slot. The microphone is placed at a distance of 0.2 m to this slot and 0.16 m above the ground (see Fig. B.2.6). The hydrophone is submerged approximately 1 m below the surface and there is 2 m from the surface of the water up to the edge of the harbour.

During the day, measurements are made of the propeller-driven high-speed craft ferry to Samsø and a speedboat with dual outboard motors both sailing around in basins 1 and 2 (see Fig. B.2.7). In the evening no specific noise sources were noticed (see Fig. B.2.8).

While conducting the measurements, the highest 10 min average wind speed was 4.7 m/s during the day and 3.3 m/s in the evening [45], and the water temperature was 6.9 °C [11].

Figure B.2.3: Nautical map of the measurement location (highlighted with a red dashed ellipse).

(a) Inward

(b) Outward

Figure B.2.4: Location overview.

(a) Overview

(b) Zoom

Figure B.2.5: Hydrophone attached to telescope pole.

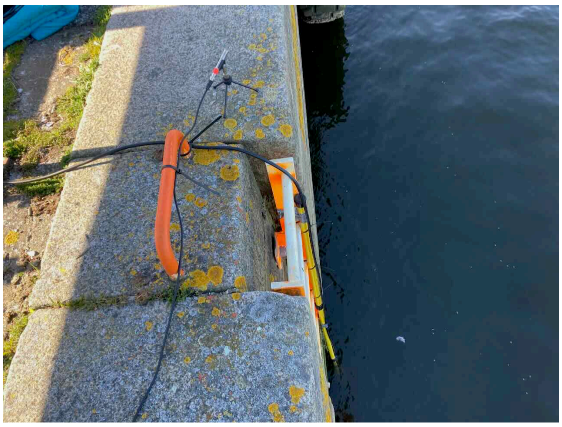

(a) Hydrophone mounting

(b) Equipment overview

Figure B.2.6: Mounting of the hydrophone and placement of equipment at the harbour.

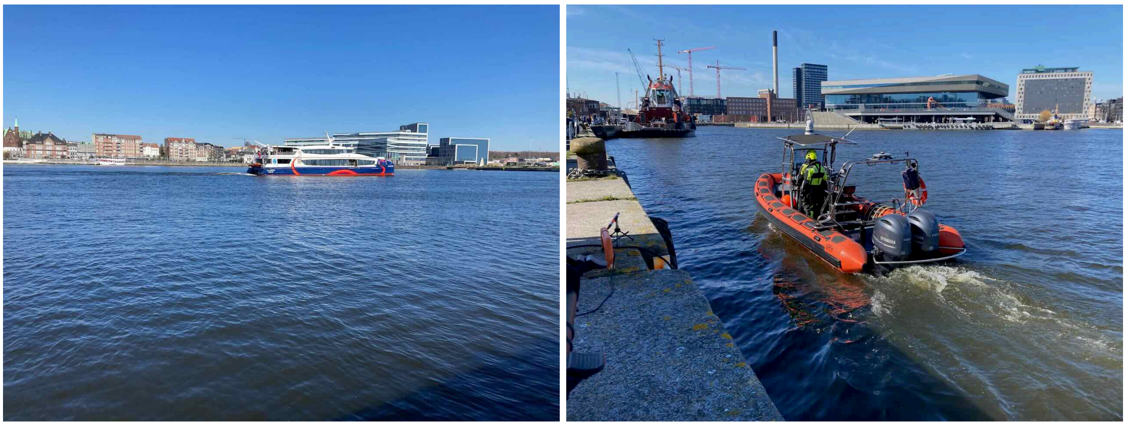

(a) Ferry to Samsø

(b) Speed boat

Figure B.2.7: Specific noise sources.

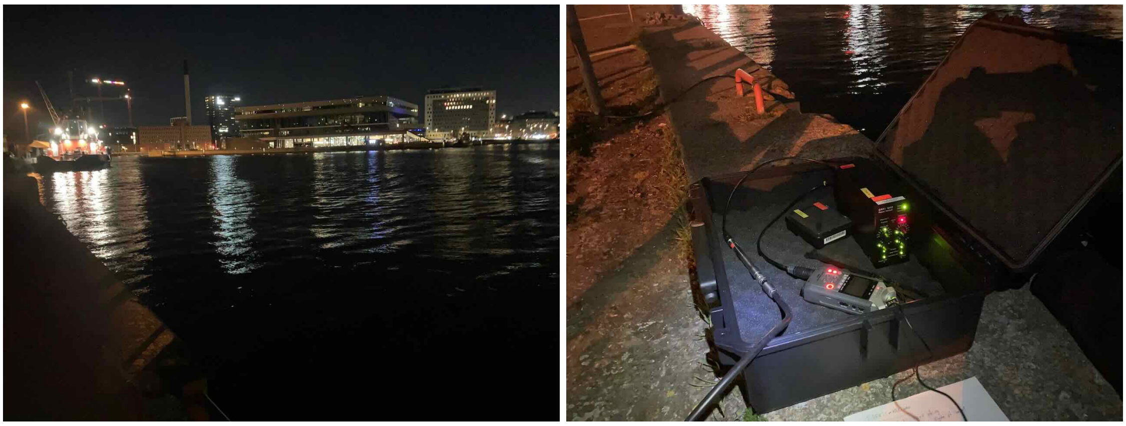

(a) Overview

(b) Setup

Figure B.2.8: Overview and setup from evening measurements.

B.2.2 Method/Procedure

All recordings are made in stereo at 48 kHz/16-bit with an input level of 30 and a power module gain of 30 dB for the hydrophone. The microphone measurements are made using an input level of 1 and a power module gain of −20 dB, however, these ended up not being used.

The following calibration procedure is performed for each hydrophone:

1. Hydrophone is inserted into the 3D-printed coupler and mounted on the pistonphone calibrator.
2. Output gain is adjusted on the power module.
3. Pistonphone calibrator is turned on.
4. Signal is recorded.

The following measurement procedure is performed:

1. Hydrophone is placed in and microphone above the water.
2. Output gains are adjusted on the power module.
3. Signals are recorded.

Background noise levels are measured during the day and evening with relatively low wind and wave activity. During the day the ferry to Samsø as well as a speed boat were recorded sailing around in the harbour basins.

B.2.3 Results

All calculations and plots are made using Python 3.9.16 [46] and the following packages:

- NumPy 1.23.5 [47]
- Matplotlib 3.7.1 [48]
- SciPy 1.10.1 [49]
- librosa 0.10.0 [50]

Measurements are calibrated using a 10 s recording of the pistonphone calibration signal at each gain setting.

Sound pressure levels (left) are calculated using a fast time weighing of 125 ms which is implemented as an exponential moving average filter. The dashed line shows the average SPL.

The spectrograms (right) presented are made with a sample rate of 48 kHz and a 4096 point FFT. This results in each frame having a duration of 85 ms and a frequency resolution of 11.7 Hz. Furthermore, a 50 % overlap is used and the spectrograms all have a 80 dB dynamic range.

The script and audio files for generating the visualisations can be found in 'Attachments/Field Measurements/Aarhus Harbour'. These selected clips from the recordings are presented in the figures below.

Background Noise

Background noises measured both during the day and in the evening are presented in Fig. B.2.9 and B.2.11.

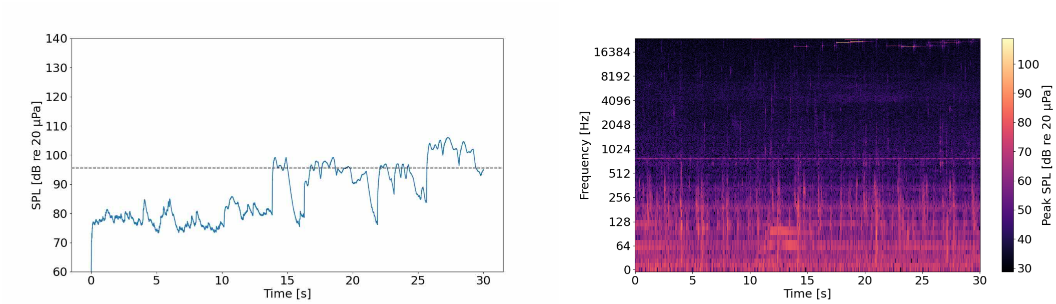

Figure B.2.9: Background noise during the day.

High-frequency tones are recorded above 18 kHz which greatly affects the broadband SPL as seen in Fig. B.2.9 from about midway. A zoomed-in plot of these tones can be seen in Fig. B.2.10. Additionally, a pulsing tone is seen and heard around 800 Hz.

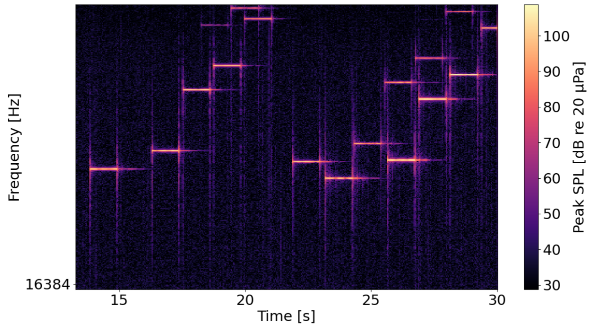

Figure B.2.10: Zoom of the high-frequency tones of the background noise during the day.

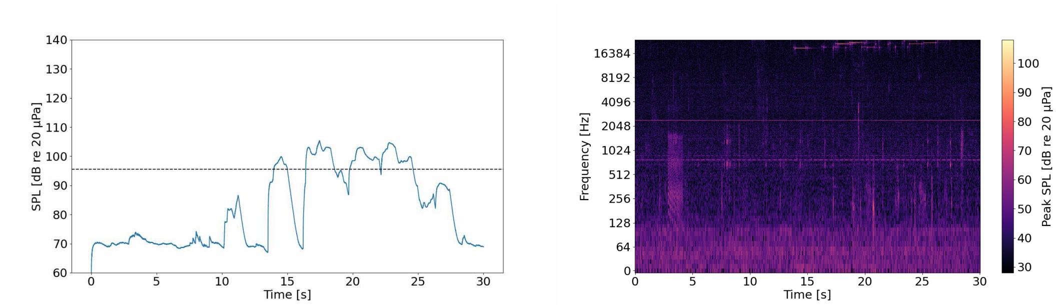

Figure B.2.11: Background noise in the evening.

The high-frequency tones are even more noticeable in the evening as seen in Fig. B.2.11 and on the zoomed plot in Fig. B.2.12. The pulsing tone is still present around 800 Hz, and a pure tone around 2400 Hz is also both visible and audible.

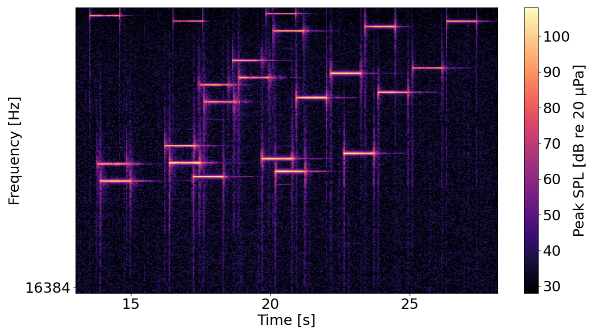

Figure B.2.12: Zoom of the high-frequency tones of the background noise in the evening.

Ferry

Measurements of the ferry arriving, idling and leaving are shown in Fig. B.2.13, B.2.14 and B.2.15.

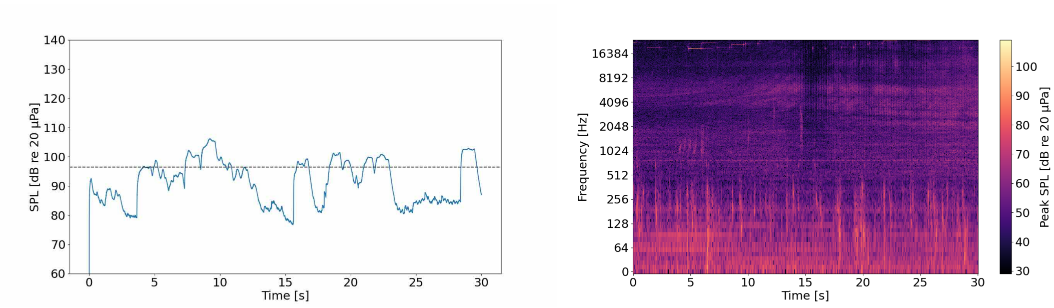

Figure B.2.13: Ferry arriving at slow speed.

With the ferry at low speed upon arrival, the high-frequency tones are still dominating as seen in Fig. B.2.13.

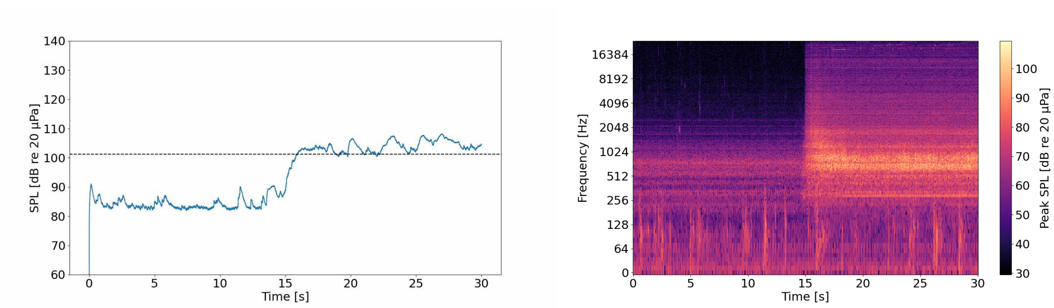

Figure B.2.14: Ferry going from idling.

Although somewhat masked by the loud engine, the high-frequency tones are still visible on the spectrogram and seen as unevenness on the SPL curve towards the end in Fig. B.2.14.

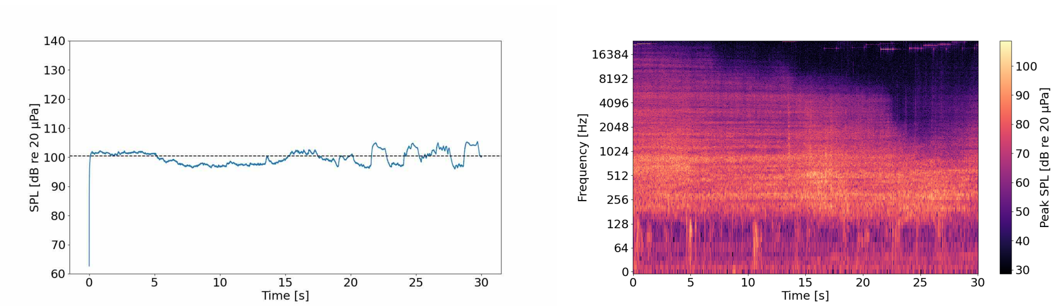

Figure B.2.15: Ferry leaving the harbour.

With the ferry leaving there are again bumps in the SPL curve and the tones are visible towards the end in Fig. B.2.15.

Bow waves, presumably created by the ferry, are captured in Fig. B.2.16 where the high-frequency tones are dominant in the first half.

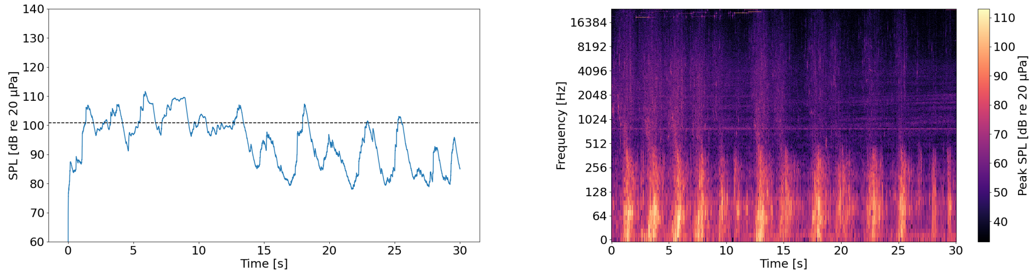

Figure B.2.16: Bow waves created by the ferry.

Speedboat

Measurements of the speedboat in the distance and close by are provided in Fig. B.2.17 and B.2.18.

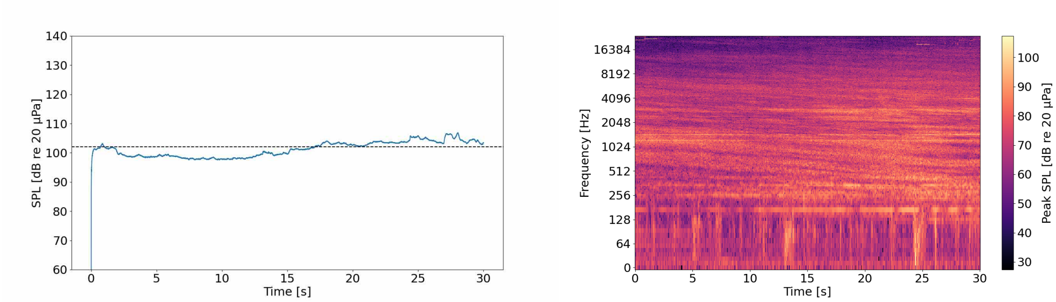

Figure B.2.17: Speedboat sailing around in the harbour.

With the speedboat both in Fig. B.2.17 and B.2.18 the high-frequency tones are still somewhat visible, however, the visual influence in these clips is minimal.

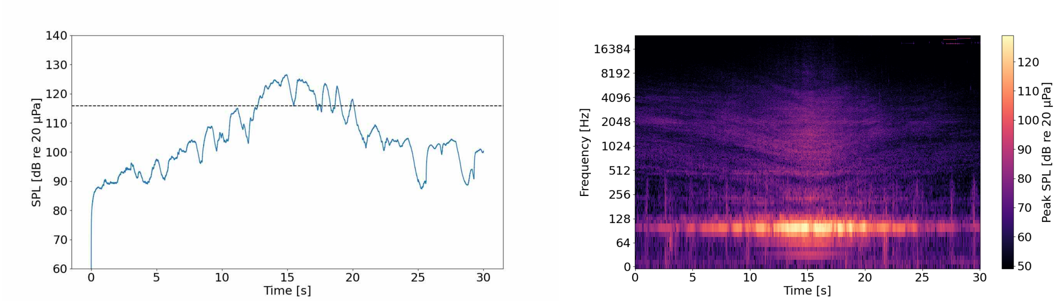

Figure B.2.18: Speedboat sailing very close by.

Touching Equipment

Deliberately handling the equipment case as well as the hydrophone cable, opposite the transducer, causes very loud noises. The long unbalanced cables are very sensitive and pick up sounds like a microphone. The spectrogram shown in Fig. B.2.19 has a greater dynamic range of 120 dB and the high-frequency tones still affect the displayed SPL.

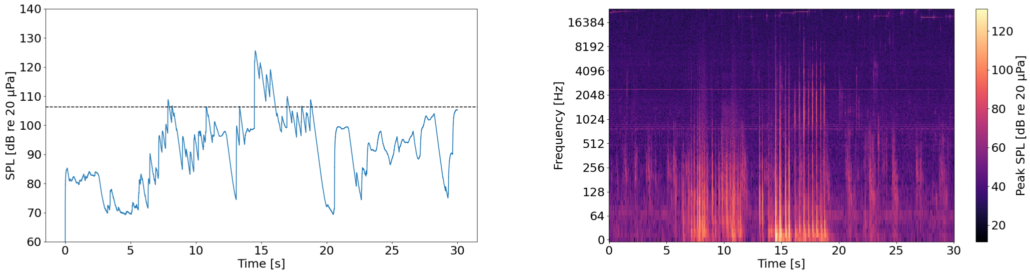

Figure B.2.19: Intentional striking of the measurement equipment.